Published OnlineFirst April 7, 2020; DOI: 10.1158/0008-5472.CAN-19-2843



# Tumor-Derived Prostaglandin E2 Promotes p50 NF-κB-Dependent Differentiation of Monocytic MDSCs

Chiara Porta[1,2], Francesca Maria Consonni[3], Sara Morlacchi[3], Sabina Sangaletti[4], Augusto Bleve[1], Maria Grazia Totaro[3], Paola Larghi[3], Monica Rimoldi[3], Claudio Tripodo[5], Laura Strauss[1], Stefania Banfi[3], Mariangela Storto[3], Tiziana Pressiani[3], Lorenza Rimassa[3], Silvia Tartari[3], Alessandro Ippolito[1], Andrea Doni[3], Giulia Soldà[3,6], Stefano Duga[3,6], Viviana Piccolo[3], Renato Ostuni[7,8], Gioacchino Natoli[3,6], Vincenzo Bronte[9], Fiorella Balzac[10], Emilia Turco[10], Emilio Hirsch[10], Mario P. Colombo[4], and Antonio Sica[1,3]

## ABSTRACT

Myeloid-derived suppressor cells (MDSC) include immature monocytic (M-MDSC) and granulocytic (PMN-MDSC) cells that share the ability to suppress adaptive immunity and to hinder the effectiveness of anticancer treatments. Of note, in response to IFNγ, M-MDSCs release the tumor-promoting and immunosuppressive molecule nitric oxide (NO), whereas macrophages largely express antitumor properties. Investigating these opposing activities, we found that tumor-derived prostaglandin E2 (PGE2) induces nuclear accumulation of p50 NF-κB in M-MDSCs, diverting their response to IFNγ toward NO-mediated immunosuppression and reducing TNFα expression. At the genome level, p50 NF-κB promoted binding of STAT1 to regulatory regions of selected IFNγ-dependent genes, including inducible nitric oxide synthase (Nos2). In agreement, ablation of p50 as well as pharmacologic inhibition of either the PGE2 receptor EP2 or NO production reprogrammed M-MDSCs toward a NOS2$^{low}$/TNFα$^{high}$ phenotype, restoring the *in vivo* antitumor activity of IFNγ. Our results indicate that inhibition of the PGE2/p50/NO axis prevents MDSC-suppressive functions and restores the efficacy of anticancer immunotherapy.

**Significance:** Tumor-derived PGE2-mediated induction of nuclear p50 NF-κB epigenetically reprograms the response of monocytic cells to IFNγ toward an immunosuppressive phenotype, thus retrieving the anticancer properties of IFNγ.

**Graphical Abstract:** http://cancerres.aacrjournals.org/content/canres/80/13/2874/F1.large.jpg.

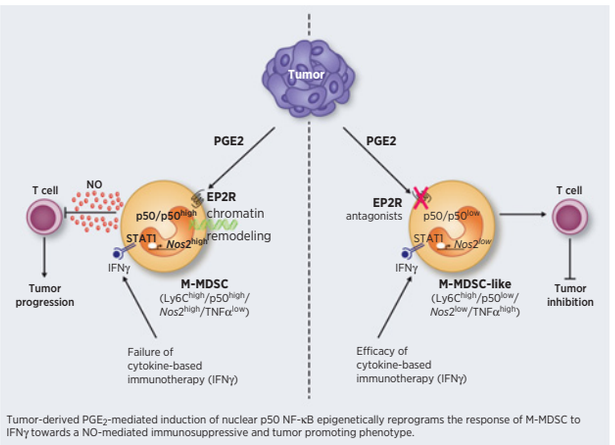


Tumor-derived $PGE_2$-mediated induction of nuclear p50 NF-κB epigenetically reprograms the response of M-MDSC to IFNγ towards a NO-mediated immunosuppressive and tumor promoting phenotype.

## Introduction

Microenvironmental signals are sensed by myeloid cells through cytokine and/or innate immune receptors, whose differential engagement leads different polarized programs (1, 2). This functional plasticity is exemplified in the M1 versus M2 extremes of macrophage polarization (1–3) and has major impacts in the orchestration of cancer-related inflammation, immunosuppression (4–6), and clinical responses (2, 7). Of note, a time-dependent M1 to M2 transcriptional reprogramming of myeloid cells was reported in response to prolonged exposure to Toll-like receptors (TLR) ligands (e.g., lipopolisaccharide; i.e., LPS tolerance; refs. 8, 9), which requires the nuclear accumulation of p50 NF-κB and results in altered responsiveness to polarizing cytokines, such as IFNγ and IL4 (9). Cancer fuels myeloid cells heterogeneity also by sustaining altered myelopoiesis (10–13) that supports resistance to anticancer immunotherapy (14). Of relevance, divergent outcomes have been reported in response to immunotherapy, either with cytokines (15–17) or checkpoint inhibitors (18, 19). In particular, IFNγ, originally termed "macrophage activating factor" (20), was paradoxically shown to be equally necessary for melanoma development and rejection (21). Indeed, IFNγ has pleiotropic and contrasting effects in the tumor microenvironment. On one hand it exerts antiangiogenic activities,

[1]Department of Pharmaceutical Sciences, Università del Piemonte Orientale "Amedeo Avogadro", Novara, Italy. [2]Center for Translational Research on Autoimmune & Allergic Diseases (CAAD) Cso Trieste 15/A, Novara, Italy. [3]Humanitas Clinical and Research Center – IRCCS, Rozzano, Milan, Italy. [4]Fondazione IRCCS Istituto Nazionale dei Tumori, Milan, Italy. [5]Human Pathology Section, Department of Health Sciences, University of Palermo, Palermo, Italy. [6]Department of Biomedical Sciences, Humanitas University, Pieve Emanuele, Milan, Italy. [7]San Raffaele Telethon Institute for Gene Therapy (SR-TIGET), IRCCS San Raffaele Scientific Institute, Milan, Italy. [8]Vita-Salute San Raffaele University, Milan, Italy. [9]Department of Medicine, Verona University Hospital, Verona, Italy. [10]Department of Molecular Biotechnology and Health Sciences, Molecular Biotechnology Center, University of Torino, Torino, Italy.

**Note:** Supplementary data for this article are available at Cancer Research Online (http://cancerres.aacrjournals.org/).

C. Porta and F.M. Consonni contributed equally to this article.

**Corresponding Author:** Antonio Sica, Università del Piemonte Orientale "Amedeo Avogadro," Department of Pharmaceutical Sciences, Largo Donegani, Novara 28100, Italy. Phone: 3903-2137-5881; Fax: 3903-2137-5621; E-mail: antonio.sica@uniupo.it

Cancer Res 2020;80:2874–88

**doi:** 10.1158/0008-5472.CAN-19-2843

Published OnlineFirst April 7, 2020; DOI: 10.1158/0008-5472.CAN-19-2843



suppression of protumorigenic properties, enhancement of tumoricidal activity of macrophages, and of processing and presentation of tumor antigens to T lymphocytes (17, 22). On the other hand, IFNγ promotes immunosuppressive functions in myeloid cells (13) inducing expression of the immunosuppressive enzymes indoleamine 2,3 dioxygenase (*Ido*) and inducible nitric oxide synthase (*Nos2*), involved in the catabolism of l-tryptophan (23) and l-arginine (12), as well as the ligand programmed-death receptor-ligand 1 (PD-L1, B7-H1; ref. 24), whose interaction with the coinhibitory receptor programmed death-1 (PD-1) can be blocked to restore antitumor immunity (25). Mixed responses to IFNγ were also reported in different human malignancies (16, 17, 26). We have previously reported that accumulation of nuclear p50 NF-κB plays an essential role in the M2 orientation of tumor-associated macrophages (TAM; refs. 9, 10), which share common myeloid precursors and a similar M2-like gene signature with M-MDSCs (10). Here, we investigated how tumor-derived signals affect transcriptional activities and myeloid cell functions in response to immune-stimulatory cytokines and the impact of these events on cytokine-mediated cancer immunotherapy.

## Materials and Methods

### Mice and ethics statement

The study was designed in compliance with Italian Governing Law (Legislative Decree 116 of January 27, 1992); EU directives and guidelines (EEC Council Directive 86/609, OJ L 358, 12/12/1986); Legislative Decree September 19, 1994, no. 626 (89/391/CEE, 89/654/CEE, 89/655/CEE, 89/656/CEE, 90/269/CEE, 90/270/CEE, 90/394/CEE, 90/679/CEE); the NIH Guide for the Care and Use of Laboratory Animals (1996 edition). All experiments involving animals described in this study were approved by the Ministry of Health (authorization numbers 160/2012-B and 25/2018-PR). The study was approved by the scientific board of Humanitas Clinical and Research Center. Mice were monitored daily and euthanized when they displayed excessive discomfort. p50 NF-κB-deficient mice on the C57BL/6J background were available in the laboratory (27). The NF-κB1flox/flox ($p50^{flox}$) mice was recently generated (28). $p50^{flox}$ mice were crossed with B6.Cg-Tg (Tek-Cre)1Ywa mice (Jackson Laboratories) to generate $p50^{flox}$; Tie2Cre mice ($p50^{Tie2}$ mice). OT-I mice were obtained from Jackson Laboratories.

### Tumor models

Eight-week-old mice were injected intramuscularly in the left leg with $10^5$ cells of murine fibrosarcoma (MN/MCA1) or subcutaneously with $5 \times 10^5$ cells of murine melanoma (B16). Tumor growth was monitored three times a week with a caliper. Bone marrow (BM) transfer and schedule of treatments are described in the Supplementary Materials and Methods

### MDSC purification

MDSC purification from the spleens of tumor-bearing mice has been performed by magnetic separation (MACS, Miltenyi Biotec; ref. 11), as described in the Supplementary Materials and Methods.

### Cell culture and reagents for mouse studies

BM-MDSCs were derived from BM cells isolated from C57BL/6 mice as described previously (29) and reported in the Supplementary Materials and Methods. Peritoneal exudate macrophages (PEC) were obtained as described previously (10). Preparation of MN/MCA1 tumor supernatant (TSN) and reagents used for mouse studies are described in the Supplementary Materials and Methods.

### Cell culture and reagents for human studies

Human monocytes were isolated from peripheral blood as described previously (9) and cultured in RPMI1640 containing 10% FBS, 2 mmol/L glutamine, 100 U/mL penicillin–streptomycin. Culture of human pancreatic carcinoma cell line PANC1 and preparation of tumor-conditioned supernatant (TSN) are described in the Supplementary Materials and Methods.

The concentration for the different treatments were as follows: PANC1 supernatant (30%), human IFNγ (PeproTech) 20 ng/mL, prostaglandin E2 (PGE2) receptor (EP2/EP1) antagonist AH6809 (Tocris) $10^{-5}$ mol/L.

### Nitrite production

A total of $2 \times 10^5$ cells were plated and stimulated with IFNγ (PeproTech, 200 U/mL) for indicated time points. Nitric oxide production was evaluated in culture supernatant using the Griess Reagent System (Promega) as described in Supplementary Materials and Methods.

### Suppression assay

M-MDSCs ($CD11b^+Ly6C^+Ly6G^-$ cells) and PMN-MDSCs ($CD11b^+Ly6C^{low/-}Ly6G^+$ cells) were isolated from spleen and tumor of wild-type (WT) and $p50^{-/-}$ MN-MCA1 tumor-bearing mice. A total of $2 \times 10^5$ splenocytes from naive C57Bl6 mice were labelled with 1 μmol/L CFSE and then cocultured with $1 \times 10^5$, $5 \times 10^4$ or $2.5 \times 10^4$ WT M-MDSCs, in the presence of anti-CD3 (3 μg/mL, 2C11, BioLegend) and anti-CD28 (2 μg/mL, 37.5; BD Biosciences). Similarly, M- and PMN-MDSC from WT and $p50^{-/-}$ mice were stimulated with IFNγ (200 U/mL) for 3 days and then cocultured with activated CFSE-labeled splenocytes. After 3 days of coculture, cells were stained and CFSE signal of gated lymphocytes was used to analyze cell proliferation. For antigen-specific suppression assay, mixed-lymphocyte reaction was performed as reported previously (11). M-MDSCs isolated from the spleen of tumor-bearing mice were then stimulated with IFNγ (200 U/mL), in the presence or absence of 500 μmol/L of L-NG-monomethylarginine (L-NMMA; Calbiochem). At day 3, 50 μL of supernatant was tested for nitric oxide (NO) production (as control) and $2 \times 10^5$ splenocytes from OT-I mice were added for additional 72 hours in the presence of 250 μg/mL of ovalbumin peptide (OVA257–264; Sigma). [3H] thymidine was added for the last 16 hours of culture and its incorporation was analyzed by MicroBeta plate counter (Perkin Elmer). As controls, OT-1 splenocytes alone were pulsed with OVA peptide (250 μg/mL) or kept in culture media. All conditions were evaluated in triplicates.

### Isolation of MDSCs from patients with colorectal cancer

The study was conducted in accordance with recognized ethical guidelines (Declaration of Helsinki) was approved by the Institute Ethical Committee, and written informed consent was obtained from 20 patients. Twenty milliliters of peripheral blood were collected from healthy donors and patients with T2 or T3 colorectal cancer. Patients with colorectal cancer did not receive radiation or chemotherapy before sample collection. Blood was stratified on Ficoll gradient to separate peripheral blood mononuclear cells (PBMC). All blood samples were analyzed within 3 hours after collection by FACS analysis. Briefly, $1 \times 10^6$ cells were resuspended in Hank's Balanced Salt Solution (HBSS; Lonza) supplemented with 0.5% BSA (Sigma).

Published OnlineFirst April 7, 2020; DOI: 10.1158/0008-5472.CAN-19-2843



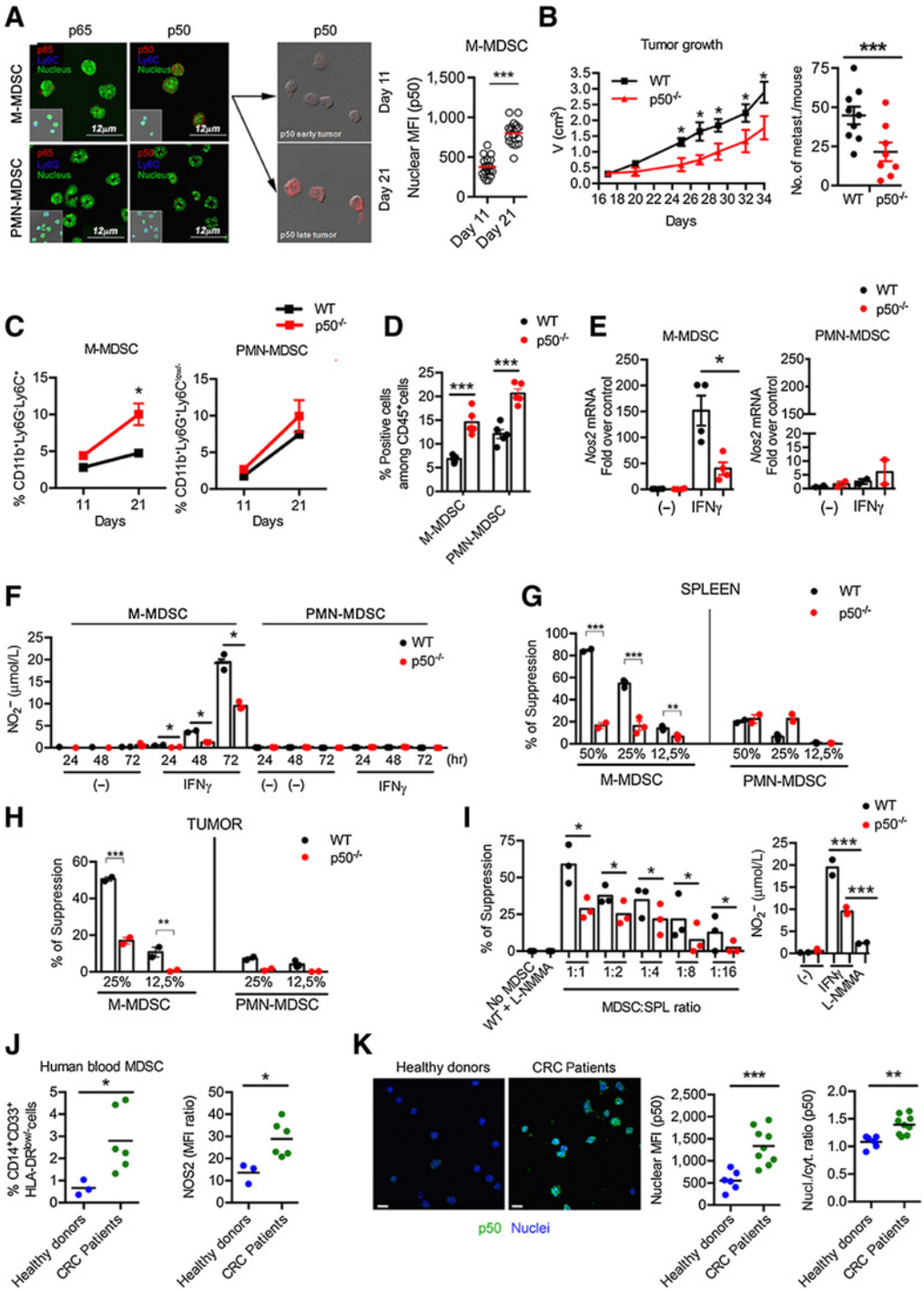


**Figure 1.**

Role of p50 NF-κB in IFNγ-induced NO-dependent suppressive activity of M-MDSC. **A,** Left, confocal microscopy showing selective upregulation of nuclear p50 NF-κB in the splenic M-MDSC subset during tumor growth (day 21). **A,** Right, quantification of p50 nuclear accumulation (***, $P < 0.001$ by two-tailed $t$ test; $n = 19$ nuclei of M-MDSC day 11; $n = 18$ nuclei of splenic M-MDSC day 21). **B,** Inhibition of both tumor growth (MN/MCA1; data shown are mean ± SD; *, $P < 0.01$ by two-tailed two-way ANOVA; $n = 9$ WT and $n = 8$ p50$^{-/-}$ mice) and metastasis formation in p50 NF-κB–deficient mice (data shown are mean ± SEM; ***, $P < 0.001$ by two-tailed $t$ test; $n = 9$ WT and $n = 8$ p50$^{-/-}$ mice). **C** and **D,** Increased number of M-MDSCs (CD11b$^{+}$Ly6G$^{-}$Ly6C$^{+}$ cells) in the spleen (**C**) and in the tumor (**D**) of p50$^{-/-}$ tumor-bearing mice (data shown are mean ± SEM; *, $P < 0.05$ by two-tailed two-way ANOVA; $n = 5$ WT and $n = 5$ p50$^{-/-}$ mice). **E,** Lack of p50 in M-MDSC impairs *Nos2* mRNA expression in response to IFNγ (data shown are mean ± SEM; ***, $P < 0.001$, by two-tailed $t$ test; $n = 4$ WT M-MDSCs and $n = 4$ p50$^{-/-}$ M-MDSCs; $n = 2$ WT PMN-MDSCs and $n = 2$ p50$^{-/-}$ PMN-MDSCs biological replicates each run in triplicate). (*Continued on the following page.*)

Published OnlineFirst April 7, 2020; DOI: 10.1158/0008-5472.CAN-19-2843



Staining was performed at 4°C for 30 minutes, with a cocktail of mAbs to HLA-DR-Pacific Blue (clone L243); CD14-PE, -APC, -FITC (clone M5E2); CD33-PerCp-Cy5.5 (clone WM53); iNOS/NOS Type II-FITC (Clone 6/iNOS/NOS Type II), from BD Biosciences or BioLegend. Furthermore, we used unconjugated rabbit monoclonal anti-human EP2R [clone EPR8030(B); Abcam] followed by incubation with secondary goat anti-rabbit Alexa Fluor 488–conjugated antibody (Life Technologies). For intracellular staining, Foxp3/Transcription Factor Staining Buffer Set (eBioscence) were used according to the manufacturer's instructions. Cells were analyzed using the BD FACSCanto II or BD LSRFortessa and BD FACSDiva and FlowJo (9.3.2) software. When needed, cells were stained, sorted using a BD FACSAria III cell sorter, and subsequently analyzed by confocal microscopy.

### BM colony formation

BM cells were isolated from the tibias and femurs of WT or $p50^{-/-}$ mice and the colony formation capacity was measured by detection and quantification using MethoCult GF M3434, which supports optimal growth of granulocyte–macrophage progenitors (CFU-GM, CFU-M, CFU-G), of erythroid progenitors (BFU-E) and multipotential granulocyte, erythroid, macrophage, megakaryocyte progenitors (CFU-GEMM). Twelve days after seeded, colonies were counted independently by two separate operators.

### Histopathologic analysis of mice BM

Sections of WT and $p50^{-/-}$ BM were routinely stained with hematoxylin and eosin and analyzed by an expert pathologist (C. Tripodo) using a Leica DM2000 optical microscope (×400 and ×630 magnification) and microphotographs were collected with a Leica DFC320 digital camera using the Leica IM50 imaging software.

### Quantification of circulating granulocytes in peripheral blood smears

Cell counts were visually performed on five May–Grunwald Giemsa-stained smears on high-power microscopic fields (×400 magnification) and the average number of total and immature granulocytes was determined by averaging the counts.

### Flow cytometry and sorting

Splenocytes were collected from spleen after disaggregation and filtration through Falcon strainers (70 μm). Primary tumors were cut into small pieces, disaggregated with 0.5 mg/ml collagenase IV and 150 U/ml DNase I in RPMI1640 for 30 minutes at 37°C and filtered through strainers. Cells ($10^6$) were resuspended in HBSS (Lonza) supplemented with 0.5% BSA (Sigma) and the staining was performed at 4°C for 20 minutes with specific antibodies (detailed information is provided in the Supplementary Materials and Methods). Cells were analyzed using the BD FACSCanto II or BD LSRFortessa and BD FACSDiva and FlowJo (9.3.2) software.

### mRNA Sequencing

Total RNA was extracted from 1–5 × $10^6$ M-MDSC (RNeasy kit, Qiagen), and 2–5 μg were used to generate sequencing libraries with a Truseq RNA Sample Prep Kit V2 (Illumina) according to the manufacturer's instructions. Sequencing was performed on a HiSeq2000 (Illumina).

### Chromatin immunoprecipitation

Chromatin immunoprecipitation (ChIP) was carried out with a previously described high-throughput protocol (30, 31). Details are reported in the Supplementary Materials and Methods.

### Computational methods

Computational analysis of data generated by RNA sequencing (RNA-seq) and ChIP-seq is described in the Supplementary Experimental Procedures.

### Confocal microscopy on BM-MDSCs, spleen MDSCs, and PECs

Cells were seeded on Poly-L-lysine (Sigma-Aldrich) coated sterile rounded glasses at 2 × $10^5$ cells/mL in medium and fixed with 4% PFA for 10 minutes at room temperature. Cell staining and analysis are described in Supplementary Material and Methods.

### Statistical analysis

Statistical significance between two groups was determined by two-tailed Student *t* test or two-way ANOVA corrected for multiple comparison by Sidak test and among more than two groups by one-way or two-way ANOVA corrected for multiple comparison by Tukey test (Prism version 6). *, $P < 0.05$; **, $P < 0.01$; ***, $P < 0.001$.

Real-time PCR analysis, MTT assay, ELISA are described in the Supplementary Materials and Methods

## Results

### p50 NF-κB controls both M-MDSC–suppressive functions and differentiation of myeloid precursors

Nuclear accumulation of p50 NF-κB, as occurring in TAMs and LPS-tolerant macrophages, impairs both M1 polarization and antitumor activities (9, 10). Similar to TAMs, confocal microscopy analysis showed selective nuclear accumulation of p50 NF-κB in splenic and tumor-infiltrating monocytic (M)-MDSCs ($CD11b^+Ly6G^-Ly6C^+$ cells) from fibrosarcoma (MN/MCA1)-bearing mice, at advanced stages of tumor development (day 21; **Fig. 1A**; Supplementary Fig. S1A). As inhibition of T-cell proliferation validated the suppressive activity of these cells (Supplementary Fig. S1B), we explored whether p50 NF-κB could be actually involved in accumulation of suppressive M-MDSCs occurring during tumor development. According to our previous findings (10, 27), C57BL/6 $p50^{-/-}$ mice displayed both reduced tumor growth and metastasis formation, as

(*Continued.*) **F,** Reduced IFNγ-mediated NO production in $p50^{-/-}$ M-MDSCs (data shown are from a representative experiment; *, $P < 0.05$ by two-tailed t-test; $n = 3$ WT and $n = 3$ $p50^{-/-}$ technical replicates). **G** and **H,** Both spleen (**G**) and tumor (**H**) $p50^{-/-}$ M-MDSCs showed a decreased ability to inhibit T-cell proliferation in response to IFNγ at different MDSC: splenocytes ratio (data shown are from a representative experiment; *, $P < 0.05$; ***, $P < 0.001$ by two-tailed *t* test; $n = 3$ WT and $n = 3$ $p50^{-/-}$ technical replicates). **I,** Left, decreased antigen-specific suppressive activity of $p50^{-/-}$ M-MDSCs in response to IFNγ at different MDSC:OT1 splenocytes ratio (data shown are from a representative experiment; *, $P < 0.05$; ***, $P < 0.001$ by two-tailed *t* test; $n = 3$ WT and $n = 3$ $p50^{-/-}$ technical replicates). Right, decreased NO production in the coculture supernatants of IFNγ-treated $p50^{-/-}$ M-MDSCs, as compared with WT M-MDSCs. L-NMMA, nitric oxide synthase inhibitor (data shown are from a representative experiment; *, $P < 0.05$; ***, $P < 0.001$ by two-tailed *t* test; $n = 2$ technical replicates). **J,** Left, increased number of $CD33^+CD14^+HLA\text{-}DR^{low/-}$ cells in blood from patients with colorectal cancer. Right, NOS2 expression from $CD14^+$ and $CD14^+HLA\text{-}DR^{low/-}CD33^{++}$ cells in blood from healthy donors and patients with colorectal cancer (*, $P < 0.05$ by two-tailed *t* test; $n = 3$ healthy donors; $n = 6$ patients with colorectal cancer). **K,** Left, representative confocal microscopy on nuclear p50 in peripheral blood $CD14^+HLA\text{-}DR^{low/-}$ cells from patients with colorectal cancer (CRC), as compared with peripheral blood mononuclear $CD14^+$ cells from healthy donors. Scale bars, 10 μm. Right, mean fluorescence intensity (MFI) of nuclear and nuclear versus cytoplasmic ratio of p50 in $CD14^+HLA\text{-}DR^{low/-}$ cells from patients with colorectal cancer ($n = 6$ healthy donors; $n = 9$ patients with colorectal cancer). **, $P < 0.01$; ***, $P < 0.001$ by two-tailed *t* test.

Published OnlineFirst April 7, 2020; DOI: 10.1158/0008-5472.CAN-19-2843



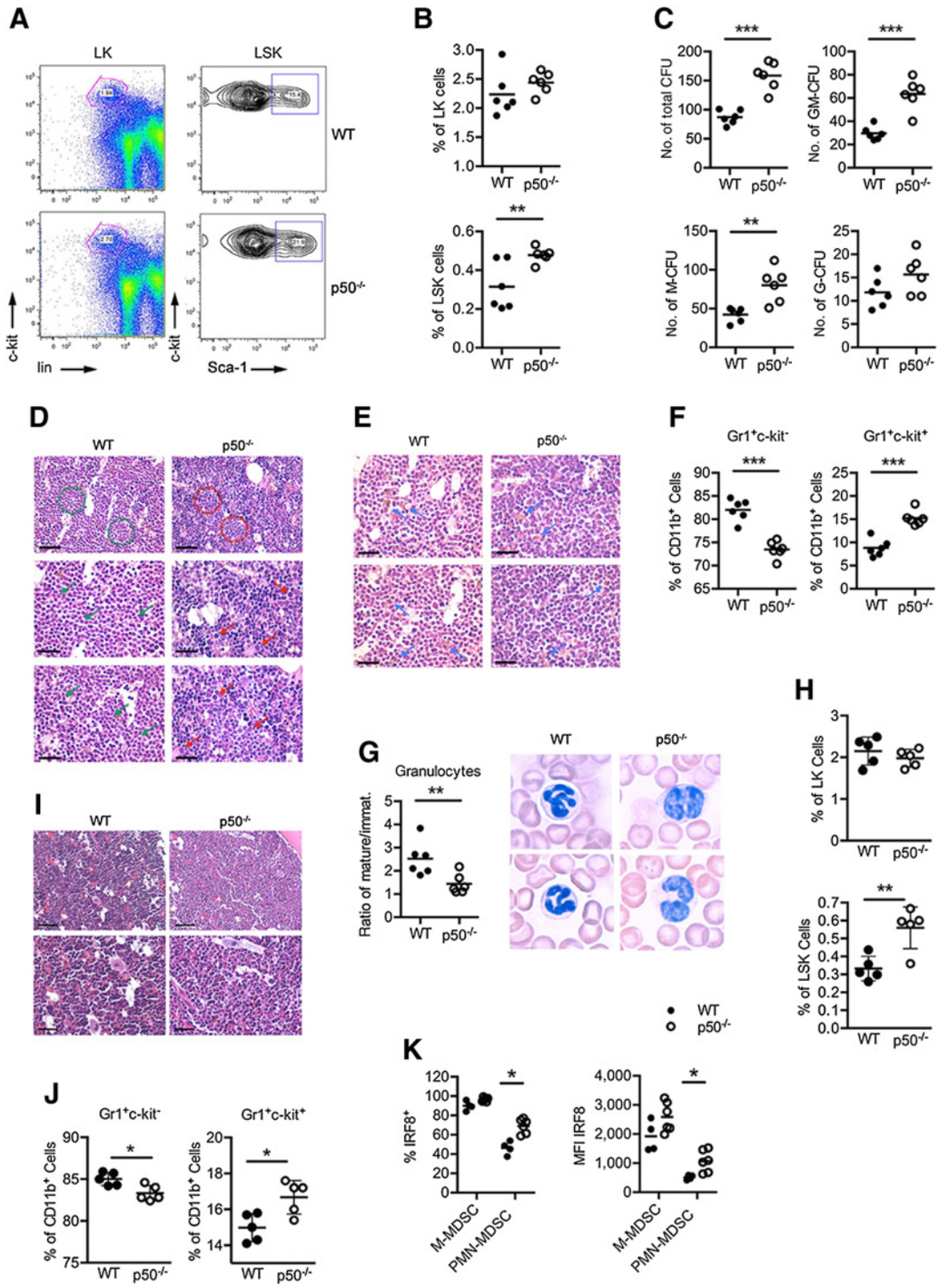


**Figure 2.**

p50 deficiency in the BM stroma associates with enhanced myelopoiesis. BM cells from WT and p50$^{-/-}$ mice were stained with mAb to c-Kit, Sca-1, and lineage- specific markers (CD3, CD11b, CD11c, Gr-1, B220, ter119). LSK progenitors were defined as Sca1$^{+}$ cells within the gate of lin$^{-}$c-Kit$^{+}$ cells. **A,** Representative FACS analysis of LSK progenitors in WT and p50$^{-/-}$ BM. **B,** Collective data showing that the fraction of LSK progenitors is increased in p50$^{-/-}$ mice ($n = 6$ WT and $n = 6$ p50$^{-/-}$ mice). **C,** Hematopoiesis was analyzed using a clonogenic colony culture assay. The relative number of total BM-CFU, GM-CFU, and M-CFU myeloid colonies was significantly increased in p50$^{-/-}$ mice compared with the WT counterpart. ($n = 6$ WT and $n = 6$ p50$^{-/-}$ mice). **D,** Histopathologic analysis (hematoxylin and eosin) of the BM of p50$^{-/-}$ and control WT mice. The BM hematopoietic parenchyma of p50$^{-/-}$ mice is characterized by the marked impairment of terminal granulopoiesis and by the increase in the density of immature myeloid precursors and blasts that show aggregation in clusters. (*Continued on the following page.*)

Published OnlineFirst April 7, 2020; DOI: 10.1158/0008-5472.CAN-19-2843



compared with WT mice (**Fig. 1B**) but, paradoxically, displayed increased accumulation of splenic and tumor myeloid cells expressing the M-MDSC phenotype CD11b$^+$Ly6G$^-$Ly6C$^+$ (**Fig. 1C** and **D**; Supplementary Fig. S1C). Of note this event coincided temporally with the nuclear accumulation of p50, as observed in WT mice (21 days; **Fig. 1A**). Cells expressing the PMN-MDSCs phenotype CD11b$^+$Ly6G$^+$Ly6C$^{low/-}$ also accumulated during disease progression (**Fig. 1C** and **D**; Supplementary Fig. S1C); however, without exhibiting nuclear accumulation of p50 NF-κB (**Fig. 1A**; Supplementary Fig. S1A). Hence, we analyzed whether p50 could affect the expression of genes encoding for immunosuppressive activities (12, 32). Noteworthy, in the absence of p50, magnetically sorted splenic CD11b$^+$Ly6G$^-$Ly6C$^+$ cells (Supplementary Fig. S1D) showed a drastic reduction of both *Nos2* gene expression (**Fig. 1E**) and NO production (**Fig. 1F**), in response to IFNγ treatment. Accordingly, p50 depletion impaired *in vivo* NO production in tumor tissues (Supplementary Fig. S1E). In contrast, both *Nos2* mRNA (**Fig. 1E**) and NO production (**Fig. 1F**) were poorly induced by IFNγ treatment in both WT and p50$^{-/-}$ splenic CD11b$^+$Ly6G$^+$Ly6C$^{low/-}$ cells (Supplementary Fig. S1D). Furthermore, the expression of arginase I (*Arg1*; ref. 13), indoleamine-2,3-dioxygenase (*Ido1*), and programmed cell death 1 ligand 1 (*CD274*) were poorly affected by the lack of p50 in both splenic and tumor CD11b$^+$Ly6G$^-$Ly6C$^+$ and CD11b$^+$Ly6G$^+$Ly6C$^{low/-}$ cells (Supplementary Fig. S1F and S1G) and not further investigated. To establish the actual role of p50 NF-κB in the suppressive activity of both myeloid subsets, CD11b$^+$Ly6G$^-$Ly6C$^+$ and CD11b$^+$Ly6G$^+$Ly6C$^{low/-}$ cells were isolated from tumor and spleen of fibrosarcoma (MN/MCA1)-bearing mice, activated with IFNγ and tested for their ability to inhibit T-cell proliferation. Consistently, both splenic and tumor M-MDSCs from WT mice strongly inhibited T-cell proliferation, whereas the p50-deficient counterparts displayed impaired suppressive ability (**Fig. 1G** and **H**).

In accordance with the lack of p50 nuclear accumulation, CD11b$^+$Ly6G$^+$Ly6C$^{low/-}$, both WT and p50-deficient, showed no suppressive activity (**Fig. 1G** and **H**). To further characterize the mechanisms underpinning the suppressive activity of p50 NF-κB, splenic M-MDSCs isolated from tumor-bearing mice were activated with IFNγ and tested for antigen-specific suppressive activity. In keeping with the data above, p50$^{-/-}$ M-MDSCs displayed reduced suppressive activity (**Fig. 1I**, left), and NO levels in the coculture supernatants (**Fig. 1I**, right). The M-MDSC–suppressive activity was NO-dependent, as addition of the NOS inhibitor L-NMMA to the coculture abolished both T-cell suppression (**Fig. 1I**, left) and NO production (**Fig. 1I**, right). These data suggested that the NO-dependent suppressive capacity of M-MDSCs in response to IFNγ, relies on p50 nuclear accumulation. We next determined whether the nuclear accumulation of p50 was also observable in blood M-MDSCs (13, 33) from patients with colorectal carcinoma. Compared with healthy donors, the frequency of M-MDSC (CD33$^+$CD14$^+$HLA-DR$^{low/-}$) was increased and these cells expressed higher level of NOS2 (**Fig. 1J**; Supplementary Fig. S2A), as well as increased nuclear levels of p50 (**Fig. 1K**), as compared with peripheral blood mononuclear CD14$^+$ cells from healthy donors. To confirm the role of p50 in human myeloid cells, circulating CD14$^+$HLA-DR$^+$ mononuclear cells from healthy donors were transfected with a small interfering RNA against p50 (p50 siRNA). Silencing of p50 (Supplementary Fig. S2B), significantly inhibited *Nos2* mRNA expression in response to IFNγ treatment (Supplementary Fig. S2C).

The predominant increase in the M-MDSCs subset within the spleen of tumor-bearing mice might results from its accelerated proliferation rate or preferential skewing of precursors. To study the implication of p50 in either normal or emergency hematopoiesis, we first evaluated the BM of naïve mice for composition in hematopoietic stem cells (HSC), along with their proliferation and differentiation potential. HSCs are immunophenotypically defined as cells lacking lineage specific markers (Lin−) but expressing Sca-1 and c-Kit (Lin-Sca-1+c-kit+, LSK), while the methylcellulose-based colony-forming unit (CFU) assay allows to quantify their derived progeny *in vitro*. We observed a significant enrichment of LSK progenitors (Lin-Sca-1+c-kit+) in BM of p50$^{-/-}$ mice (**Fig. 2A** and **B**), associated with higher clonogenic potential of p50$^{-/-}$ HSCs in both GM-CFU and M-CFU progenitors, but not in G-CFU (**Fig. 2C**). These results indicate that lack of p50 results in a preferential skewing of HSCs toward the monocytic branch at the myeloid/granulocytic bifurcation. Accordingly, histopathologic analysis showed a severe impairment of terminal granulopoiesis in the BM of p50$^{-/-}$ mice, which was associated with an increased number of immature myeloid precursors (**Fig. 2D**). Consistently, the hematopoietic parenchyma of p50$^{-/-}$ mice was characterized by the marked reduction of mature segmented granulocytes and by the expansion of myeloid blasts showing abnormal interstitial localization and aggregation in clusters (**Fig. 2D**). Monocytic differentiation (**Fig. 2E**) was preserved in the BM of p50$^{-/-}$ mice. Consistent with BM histopathology, flow cytometry revealed a neat decrease in the Gr1$^+$c-Kit$^-$ granulocytic population and a paralleled increase in Gr1$^+$c-kit$^+$ myeloblasts in p50$^{-/-}$, as compared with control WT BM (**Fig. 2F**). Accordingly, blood granulocytes from p50$^{-/-}$ mice were enriched in immature and blast-like forms compared with circulating granulocytes from WT controls (**Fig. 2G**). Overall, these results confirm previous observations (34) and demonstrate that p50 NF-κB deficiency is associated with defective granulocytic differentiation in favor of the monocytic lineage. Lack of p50 resulted in a significant accumulation of LSK progenitors (Lin-Sca-1$^+$c-kit$^+$) also in the BM of tumor bearers (**Fig. 2H**). Furthermore, both histopathology (**Fig. 2I**) and flow cytometry (**Fig. 2J**) of BM confirmed the reduction of the mature Gr1$^+$c-kit$^-$ and the concomitant increase of the immature Gr1$^+$c-kit$^+$ granulocytic cells in p50$^{-/-}$

(*Continued.*) Red arrows, myeloid blasts. Original magnifications: top, scale bars, 100 μm; bottom, scale bars, 50 μm. **E,** Monocytic differentiation is preserved in the BM of p50$^{-/-}$ mice, as testified by the presence of cells with mature monocytic morphology and by the normal density of hemosiderin-laden macrophages. Scale bars, 50 μm. **F,** Fraction of mature Gr-1$^+$c-kit$^-$ and immature Gr-1$^+$c-Kit$^+$ granulocytes in BM from WT and p50$^{-/-}$ mice. The fraction of immature granulocytes is increased in the absence of p50 in comparison with the WT counterpart ($n$ = 6 WT and $n$ = 6 p50$^{-/-}$ mice). **G,** Morphologic analysis (left) and quantification (right) of Giemsa-stained peripheral blood smears from 12 weeks-old p50$^{-/-}$ and WT mice showing that circulating granulocytes from p50$^{-/-}$ mice are enriched in immature and blast-like forms ($n$ = 6 WT and $n$ = 6 p50$^{-/-}$ mice). **H,** Increased fraction of LSK progenitors in the BM of p50$^{-/-}$ tumor bearing mice ($n$ = 5 WT and $n$ = 5 p50$^{-/-}$ mice). **I,** Histopathologic analysis (hematoxylin and eosin) of the BM of tumor-bearing mice showed a marked impairment of terminal granulopoiesis and an increased density of immature myeloid precursors and blasts in the BM hematopoietic parenchyma of p50$^{-/-}$ mice. Original magnifications: top, scale bars, 100 μm; bottom, scale bars, 50 μm. **J,** Increased frequency of immature granulocytes (Gr1$^+$c-kit$^+$ cells) in the BM of p50$^{-/-}$ tumor-bearing mice ($n$ = 5 WT and $n$ = 5 p50$^{-/-}$ mice). **K,** Cytofluorimetric analysis of IRF8 in M- (CD11b$^+$Ly6G$^-$Ly6C$^+$ cells) and PMN-MDSC (CD11b$^+$Ly6G$^+$Ly6C$^{low/-}$ cells; WT, $n$ = 4, p50$^{-/-}$ $n$ = 6 mice). *, $P < 0.05$; **, $P < 0.01$; ***, $P < 0.001$ by two-tailed $t$ test.

Published OnlineFirst April 7, 2020; DOI: 10.1158/0008-5472.CAN-19-2843



tumor bearers. Of relevance, cytofluorimetric analysis of tumor-infiltrating MDSCs revealed a significant increase of the negative regulator of MDSC expansion IRF8 (35) expression by the p50-deficient PMN-MDSC subset ($CD11b^+Ly6G^+$ cells; **Fig. 2K**), which also acts as promoter of terminal monocytic maturation (36). This result is in agreement with the preferential expansion of nonsuppressive $Ly6C^+$ monocytic cells (M-MDSC–like) observed in tumor-bearing p50-deficient mice.

### Hematopoietic deletion of p50 NF-κB abolishes NO production by M-MDSCs and impairs metastasis formation

To establish whether the expression of p50 NF-κB in the hematopoietic compartment was uniquely responsible for the suppressive activity of M-MDSCs, we generated chimeric mice by transplanting WT or $p50^{-/-}$ BM cells into sublethally irradiated WT and $p50^{-/-}$ mice, which were subsequently implanted with the MN/MCA1 fibrosarcoma. Splenic $CD11b^+Ly6G^-Ly6C^+$ cells isolated from mice receiving $p50^{-/-}$ BM cells, and subsequently activated with IFNγ, were strongly impaired in their capacity to suppress both T-cell proliferation and NO production (**Fig. 3A**). To investigate further the *in vivo* importance of p50 in the hematopoietic compartment, we used the deleter strain B6.Cg-Tg(Tek-Cre)1Ywa to ablate p50 in all hematopoietic lineage cells ($p50^{Tie2}$ mice) (37). In agreement with **Fig. 1A** and **B**, we observed inhibition of lung metastasis formation in tumor-bearing $p50^{Tie2}$ mice, which was paralleled by an increased number of splenic and tumor-infiltrating $CD11b^+Ly6G^-Ly6C^{high}$ cells, while an increase of $CD11b^+Ly6C^{low/-}Ly6G^+$ cells was observed at the tumor site (**Fig. 3B**).

Furthermore, splenic and tumor-associated $CD11b^+Ly6G^-Ly6C^+$ cells from $p50^{Tie2}$ mice (**Fig. 3C**) showed decreased NOS2 but higher TNFα expression, associated with increased number of both splenic and tumor-infiltrating IFNγ expressing $CD4^+$ and $CD8^+$ T cells (**Fig. 3D**), these latter also expressing high levels of the cytotoxic molecule granzyme B (GZMB). Accordingly, $CD11b^+Ly6G^-Ly6C^+$ cells isolated from $p50^{Tie2}$ mice showed a reduced ability to inhibit T cells' proliferation, whereas $CD11b^+Ly6G^+Ly6C^{Low/-}$ cells lacked suppressive activity (**Fig 3E**). Of note, transplantation of B16 melanoma cells (38) in $p50^{Tie2}$ mice fully recapitulated the phenotype of the MN-MCA1 fibrosarcoma, both in terms of tumor growth (Supplementary Fig. S3A) and accumulation of splenic and tumor-infiltrating immune cells (Supplementary Fig. S3B–S3D).

### p50 influences IFNγ-induced Stat1 recruitment to a subset of p50-dependent genes

Because the absence of p50 has strongly altered the response of $CD11b^+Ly6G^-Ly6C^+$ cells to IFNγ, we further investigated this aspect. IFNγ-induced Stat1 phosphorylation (39) was not reduced in the absence of p50 (**Fig. 4A**), suggesting that downstream events occurring in $p50^{-/-}$ cells could be responsible for defective IFNγ-mediated gene expression. To directly assess this hypothesis, we generated mRNA-seq datasets of WT and $p50^{-/-}$ $CD11b^+Ly6G^-Ly6C^+$ cells, isolated from the spleen of tumor-bearing mice, treated or not with IFNγ. $p50^{-/-}$ $CD11b^+Ly6G^-Ly6C^+$ cells showed selective gene expression defects in response to IFNγ stimulation as compared with WT controls (**Fig. 4B**; Supplementary Table S1). Using cutoffs, a $\log_2$ (fold change) ≥ 1 and FDR ≤ 0.05, 15 (2.4%, cluster 2) of the 628 genes induced by IFNγ in WT $CD11b^+Ly6G^-Ly6C^+$ cells *15 (2.38%)* were down-regulated in $p50^{-/-}$ cells, whereas 16 (2.5%) were upregulated. Analysis of the generated gene profiles confirmed that p50 deficiency results in a significant impaired induction of *Nos2* (**Fig. 4C**) along with an increased induction of some IFN-inducible genes, such as *Oas1g* and *Pyhin1/Ifix*, (Supplementary Table S1). Collectively, our data highlight a specific function of p50 in controlling a subset of functionally relevant genes in response to IFNγ stimulation. Because transcriptional responses to IFNγ predominantly rely on the Stat1 transcription factor, we evaluated the recruitment of Stat1 on the *Nos2* gene using ChIP with a validated antibody directed against Stat1 (30). Lack of p50 reduced binding of Stat1 on the *Nos2* gene in $CD11b^+Ly6C^{high}$ cells under both steady-state and IFNγ treatment (**Fig. 4D**), therefore indicating that p50 controls IFNγ-dependent responses at epigenetic level.

Along with MDSCs, macrophages produce NO in response to IFNγ, which mediate either their immunosuppressive (4, 13) or tumoricidal capacity (40). Similar to M-MDSCs, in thioglycollate elicited macrophages (PEC) lack of p50 decreased *Nos2* mRNA expression and NO production in response to IFNγ (Supplementary Fig. S4A), without reducing Stat1 phosphorylation (Supplementary Fig. S4B). In further analogy with MDSCs, PECs primed with the tumor supernatant (TSN) produced higher level of NO in response to IFNγ, in a p50-dependent manner (Supplementary Fig. S4C). Moreover, transcriptional analysis (mRNA-seq) of WT and $p50^{-/-}$ PECs confirmed that $p50^{-/-}$ PECs showed selective gene expression defects in response to IFNγ (Supplementary Fig. S4D and Supplementary Table S2), including *Nos2*. On the other hand, in agreement with **Fig. 2H**, p50 deficiency resulted in an increased induction of the monopoiesis-inducing transcription factor *Irf8* (36; Supplementary Table S2). We then performed ChIP coupled to next-generation sequencing (ChIP-seq). Almost all DNA binding events occurred only after Stat1 activation (Supplementary Table S3) and positively correlated with IFNγ-induced gene expression in a statistically significant manner (Supplementary Fig. S4E), highlighting the prominent role of Stat1 as a transcriptional activator. A discrete fraction of the Stat1 cistrome was selectively affected by p50 deficiency, with an abrogation or reduction of Stat1 occupancy at 2571 sites (8.3% of all inducible peaks) in $p50^{-/-}$ PEC relative to WT controls. For instance, we confirmed that Stat1 was not efficiently recruited to either promoters or enhancers of *Nos2* gene in $p50^{-/-}$ macrophages, and this was associated with its reduced induction in response to IFNγ (Supplementary Fig. S4F). These observations were then validated at a genomic scale by computationally integrating our ChIP-seq and mRNA-seq datasets (Supplementary Table S4). As shown in Supplementary Fig. S4G, p50-dependent genes were located at shorter distances from p50-dependent Stat1 peaks than p50-independent genes. Conversely, p50-independent genes were closer to p50-independent Stat1 peaks.

These findings identify a role for p50 in controlling IFNγ-induced *Nos2* gene expression in myeloid cells, and are consistent with a model of p50-dependent assistance of Stat1 recruitment to selected p50-dependent genes in response to IFNγ treatment.

### Ablation of p50 NF-κB in M-MDSCs restores the *in vivo* antitumor activity of IFNγ

We next investigated whether increased nuclear p50 NF-κB in M-MDSCs limits cytokine-mediated immunotherapy *in vivo*. While IFNγ treatment of WT tumor-bearing mice was ineffective, the same treatment significantly reduced tumor development in $p50^{-/-}$ mice (**Fig. 5A**). Noteworthy, *in vivo* depletion of $CD4^+$ and $CD8^+$ T cells in p50 NF-κB-deficient tumor bearing mice restored tumor growth (**Fig. 5A**, center) and metastasis formation (**Fig. 5A**, right), indicating that myeloid-specific p50 NF-κB is suppressing specific antitumor immunity. Hence, to test the specific contribution of p50 to the immunosuppressive activity of M-MDSCs, $p50^{-/-}$

Published OnlineFirst April 7, 2020; DOI: 10.1158/0008-5472.CAN-19-2843



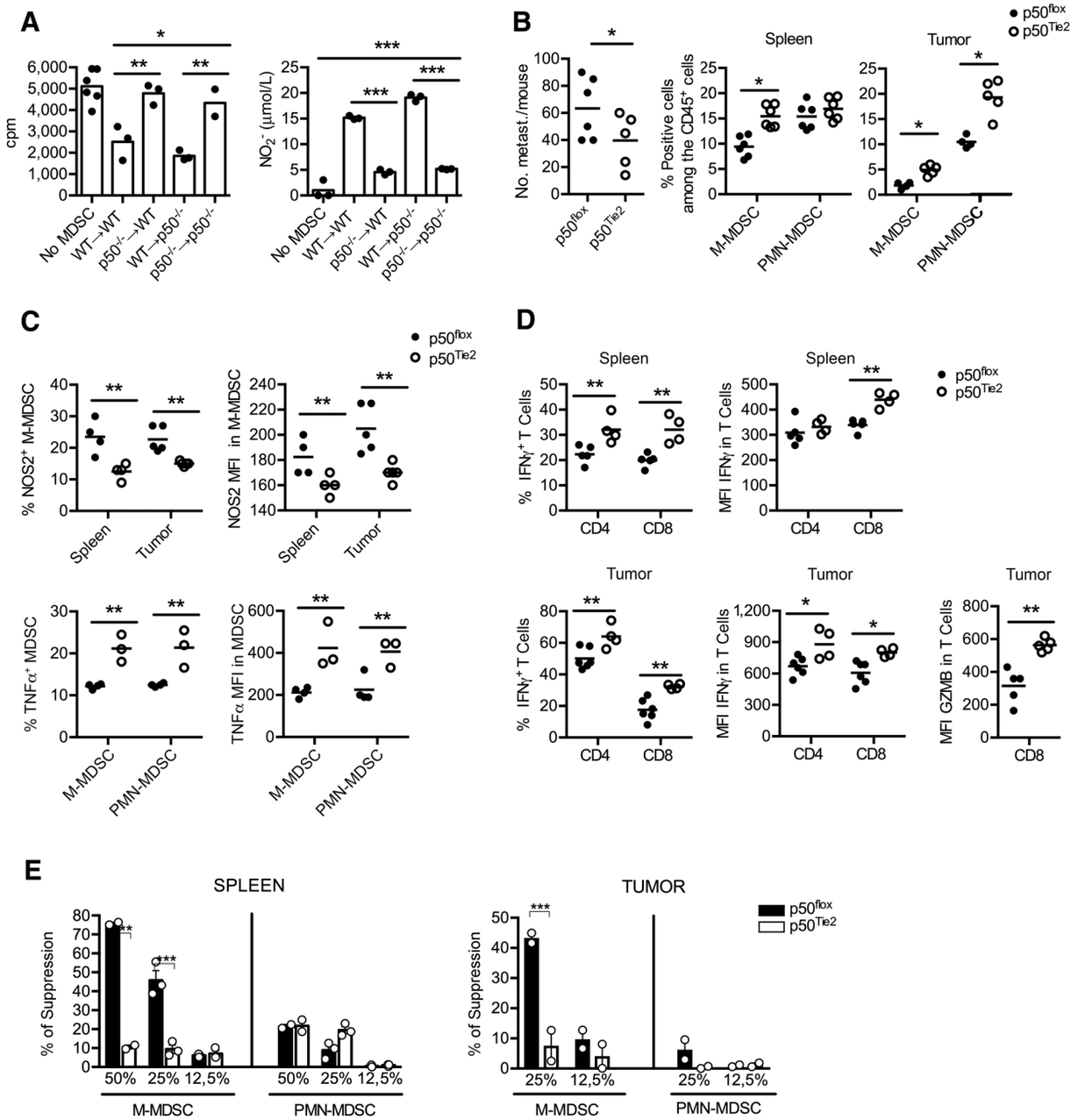


**Figure 3.**

Myeloid-specific p50 NF-κB reprograms innate ad adaptive immune functions. **A,** Splenic M-MDSC from p50$^{-/-}$ BM-transplanted mice display reduced suppressive activity (left) and NO production (right) in response to IFNγ. Proliferation was assessed by $^{3}$H-thymidine incorporation (*, $P < 0.05$; **, $P < 0.01$; ***, $P < 0.001$ by two-tailed one-way ANOVA; $n = 6$ technical replicates of T cells only; $n = 3$ technical replicates of pooled WT mice with WT BM; $n = 3$ technical replicates of pooled WT mice with p50$^{-/-}$ BM; $n = 3$ technical replicates of pooled p50$^{-/-}$ mice with WT BM; $n = 2$ technical replicates of pooled p50$^{-/-}$ mice with p50$^{-/-}$ BM). NO production by a technical triplicate ($n = 3$) for each group. ***, $P < 0.001$ by two-tailed one-way ANOVA. **B,** Left, metastasis formation in control p50$^{flox}$ and p50$^{Tie2}$ mice (*, $P < 0.05$ by one-tailed $t$ test; p50$^{flox}$ $n = 6$; p50$^{Tie2}$ $n = 5$). Center and right, increased number of splenic and tumor-infiltrating M-MDSCs (CD11b$^{+}$Ly6G$^{-}$Ly6C$^{+}$) and PMN-MDSC (CD11b$^{+}$Ly6G$^{+}$Ly6C$^{low/-}$), respectively in p50$^{Tie2}$ tumor-bearing mice (*, $P < 0.05$ by two-tailed $t$-test; spleen, $n = 6$ p50$^{flox}$ and $n = 6$ p50$^{Tie2}$ tumor-bearing mice; tumor, $n = 4$ p50$^{flox}$ and $n = 5$ p50$^{Tie2}$ mice). **C,** Top, flow cytometry analysis of NOS2 in M-MDSC from both spleen (**, $P < 0.01$ by two-tailed t-test; $n = 4$ p50$^{flox}$ and $n = 4$ p50$^{Tie2}$ tumor-bearing mice) and tumor of p50$^{flox}$ and p50$^{Tie2}$ tumor-bearing mice (**, $P < 0.01$ by two-tailed $t$-test; $n = 5$ p50$^{flox}$ and $n = 5$ p50$^{Tie2}$ mice). Bottom, flow cytometry analysis of TNFα in tumor-infiltrating M- and PMN-MDSC from p50$^{flox}$ and p50$^{Tie2}$ tumor-bearing mice (**, $P < 0.01$ by two-tailed $t$ test; $n = 4$ p50$^{flox}$ and $n = 3$ p50$^{Tie2}$ mice). **D,** Flow cytometry analysis of IFNγ- and GZMB-expressing CD4$^{+}$ and CD8$^{+}$ T cells in spleen and tumor from p50$^{flox}$ and p50$^{Tie2}$ mice (*, $P < 0.05$; **, $P < 0.01$ by two-tailed $t$ test; spleen, $n = 5$ p50$^{flox}$ and $n = 4$ p50$^{Tie2}$ tumor-bearing mice; IFNγ tumor, $n = 6$ p50$^{flox}$ and $n = 4$ p50$^{Tie2}$ mice; GZMB tumor, $n = 5$ p50$^{flox}$ and $n = 5$ p50$^{Tie2}$ mice). **E,** Inhibition of T-cell proliferation by either spleen (left) or tumor (right) p50$^{Tie2}$ M-MDSCs in response to IFNγ at different MDSC: splenocytes ratio (data shown are from a representative experiment; *, $P < 0.05$; ***, $P < 0.001$ by two-tailed $t$ test; $n = 2$ WT and $n = 2$ p50$^{-/-}$ technical replicates).

Published OnlineFirst April 7, 2020; DOI: 10.1158/0008-5472.CAN-19-2843



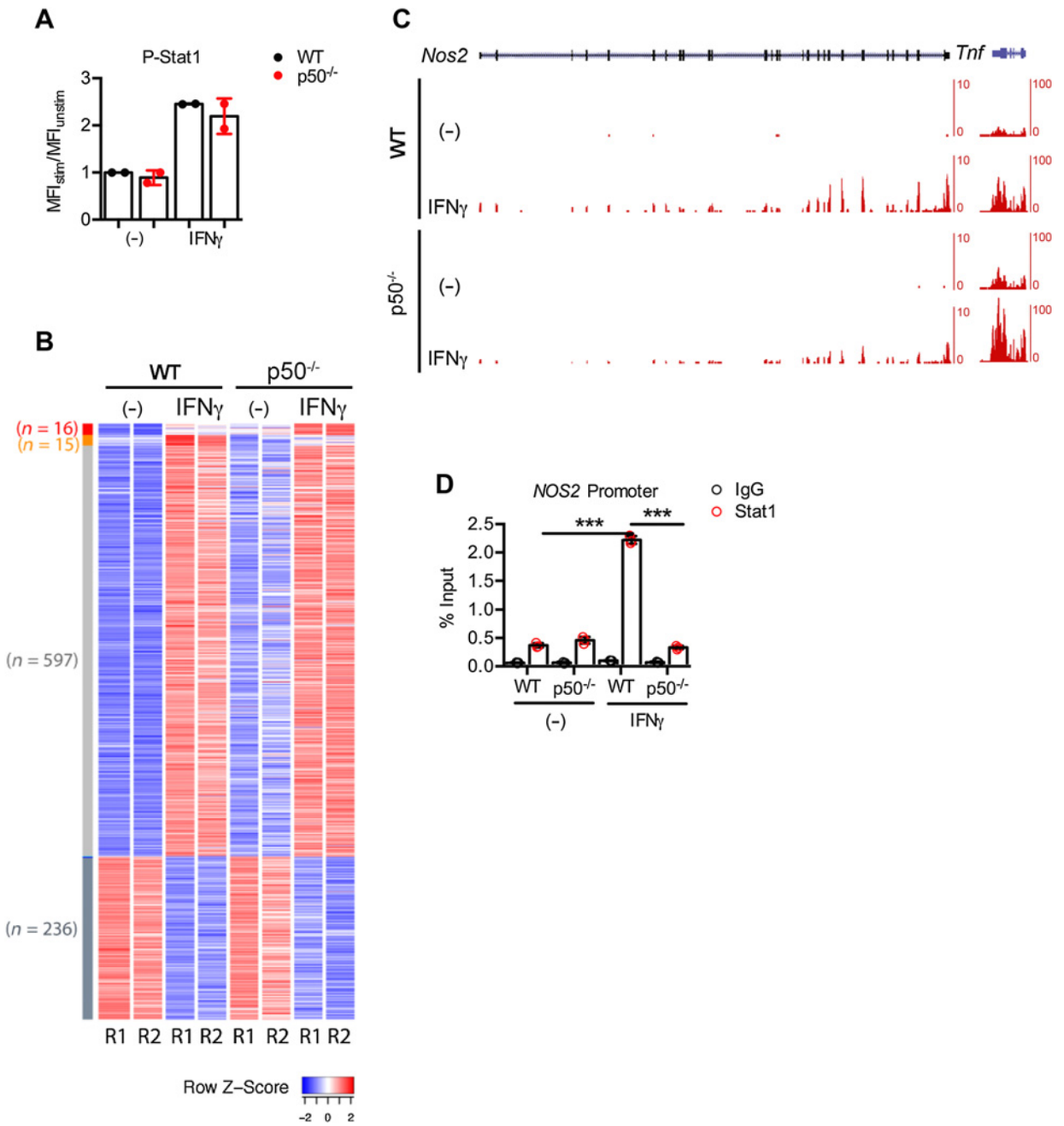


**Figure 4.**

Effects of p50 deficiency on gene expression and STAT1 binding in splenic M-MDSC from tumor-bearing mice treated with IFNγ. **A,** M-MDSC from WT and $p50^{-/-}$ tumor-bearing mice were isolated from spleen and stimulated with IFNγ for 15 minutes. Cells were stained with an anti-P-Stat1 antibody and analyzed by FACS ($n = 2$ WT and $n = 2$ $p50^{-/-}$ biological replicates). **B,** Heatmap showing selective gene expression alterations in $p50^{-/-}$ M-MDSCs stimulated with IFNγ for 4 hours ($n = 2$ WT and $n = 2$ $p50^{-/-}$ biological replicates). Data obtained with two biological replicates were highly correlated ($R^2 > 0.97$), indicating high reproducibility between samples. For each transcript, the expression level ($log_2$-transformed FPKM) is z-score scaled (red, highly expressed; blue, lowly expressed). In the vertical bar, colors indicate six groups of genes. Red, IFNγ-induced genes upregulated in $p50^{-/-}$ M-MDSCs; orange, IFNγ-induced genes downregulated in $p50^{-/-}$ M-MDSCs; light gray, IFNγ–induced genes not affected by p50 ablation; blue, IFNγ-repressed genes downregulated in $p50^{-/-}$ M-MDSCs; light blue, IFNγ–repressed genes upregulated in $p50^{-/-/-}$ M-MDSCs; gray, IFNγ-repressed genes not affected by p50 ablation. The number of genes belonging to each group is indicated on the left. **C,** A representative snapshot of RNA-seq expression data for the *Nos2* and *Tnf* genes. **D,** ChIP showing impaired recruitment of STAT1 on regulatory regions of the NOS2 promoter in splenic M-MDSCs from $p50^{-/-}$ tumor-bearing mice mice treated with IFNγ (***, $P < 0.001$ by two-tailed one-way ANOVA; $n = 3$ WT and $n = 3$ $p50^{-/-}$ technical replicates).

Published OnlineFirst April 7, 2020; DOI: 10.1158/0008-5472.CAN-19-2843



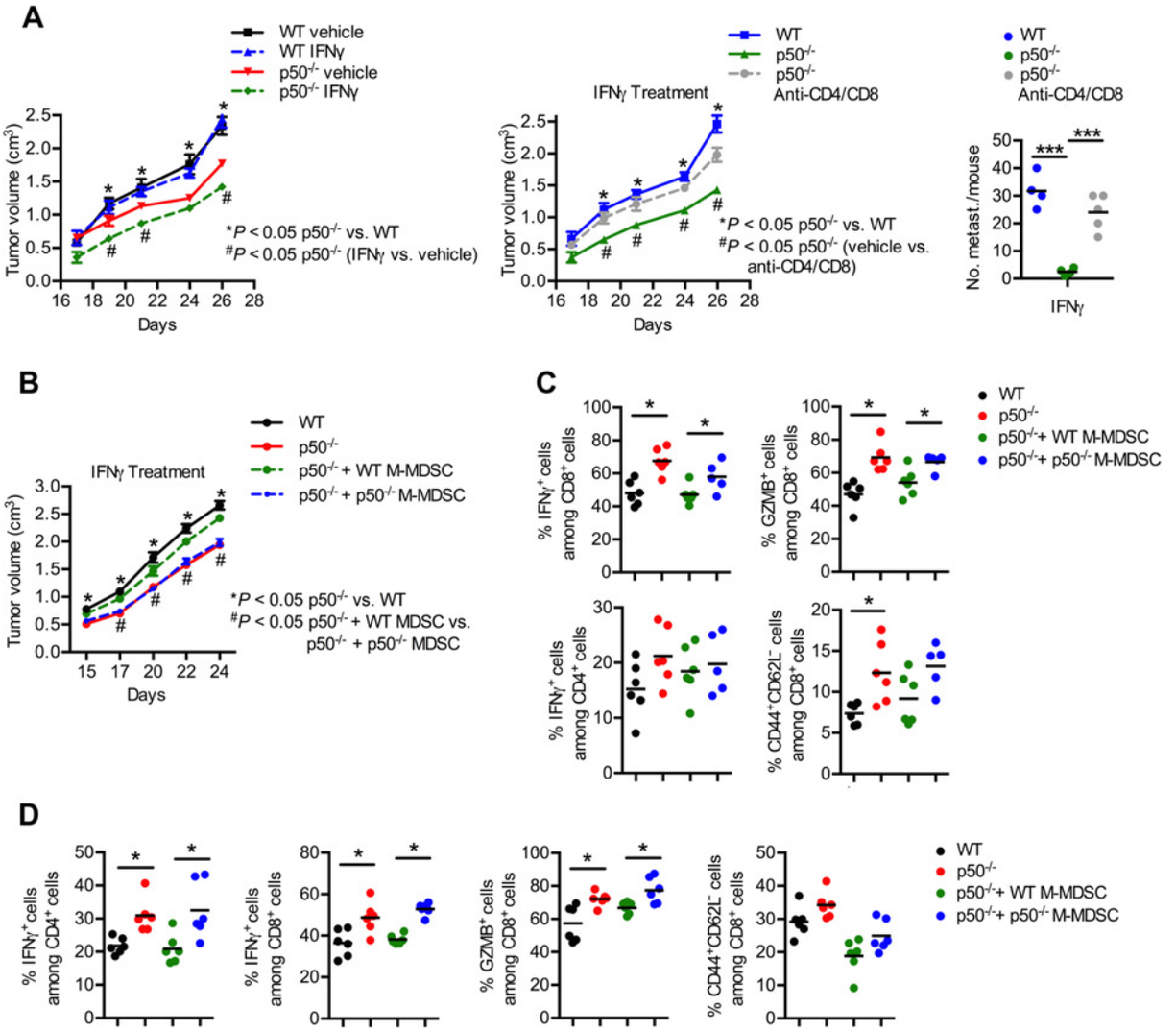


**Figure 5.**

Ablation of p50 NF-κB in M-MDSC restores IFNγ-mediated antitumor activity *in vivo*. **A,** Left, antitumor effects of IFNγ in WT versus $p50^{-/-}$ mice. Center and right, *in vivo* depletion of $CD4^+$ and $CD8^+$ T cells in p50 NF-κB-deficient tumor-bearing mice abolishes the antitumor activity of IFNγ in terms of tumor growth (data shown are mean ± SEM; *P* value was calculated by two-tailed two-way ANOVA; $n = 5$ WT vehicle-treated mice; $n = 5$ $p50^{-/-}$ vehicle-treated mice; $n = 5$ WT IFNγ-treated mice; $n = 6$ $p50^{-/-}$ IFNγ-treated mice; $n = 6$ $p50^{-/-}$ anti-CD4/CD8 and IFNγ-treated mice) and metastasis formation (***, $P < 0.001$ by two-tailed one-way ANOVA; $n = 4$ WT IFNγ-treated mice; $n = 4$ $p50^{-/-}$ IFNγ-treated mice; $n = 5$ $p50^{-/-}$ anti-CD4/CD8 and IFNγ-treated mice). **B,** Adoptive transfer of WT M-MDSC in $p50^{-/-}$ tumor-bearing mice abolishes the antitumor activity of IFNγ *in vivo*, restoring tumor growth. Data shown are mean ± SEM; *P* value was calculated by two-tailed two-way ANOVA; $n = 8$ WT mice, $n = 8$ $p50^{-/-}$ mice; $n = 7$ $p50^{-/-}$ + WT M-MDSC mice; $n = 6$ $p50^{-/-}$ + $p50^{-/-}$ M-MDSC mice. **C** and **D,** FACS analysis of $CD4^+$ and $CD8^+$ T cells for IFNγ and GZMB expression and effector memory phenotype ($CD62L^-CD44^+CD8^+$ T cells) in both spleens (*, $P < 0.05$, by two-tailed one-way ANOVA; $n = 6$ WT mice; $n = 6$ $p50^{-/-}$ mice; $n = 6$ $p50^{-/-}$ + WT M-MDSC mice; $n = 5$ $p50^{-/-}$ + $p50^{-/-}$ M-MDSC mice; **C**) and tumor (*, $P < 0.05$, by two-tailed one-way ANOVA; $n = 6$ WT mice; $n = 6$ $p50^{-/-}$ mice; $n = 6$ $p50^{-/-}$ + WT M-MDSC mice; $n = 6$ $p50^{-/-}$ + $p50^{-/-}$ M-MDSC mice; **D**) of tumor-bearing mice. WT, WT mice; $p50^{-/-}$, $p50^{-/-}$ mice; $p50^{-/-}$ + WT M-MDSC, $p50^{-/-}$ mice adoptively transferred with WT M-MDSC; $p50^{-/-}$ + $p50^{-/-}$ M-MDSC, $p50^{-/-}$ mice adoptively transferred with $p50^{-/-}$ M-MDSCs.

tumor-bearing mice were adoptively transferred with WT M-MDSCs ($1 \times 10^6$) and treated daily with IFNγ. Such M-MDSCs transfer restored tumor growth in $p50^{-/-}$ mice (**Fig. 5B**) and decreased both IFNγ production and GZMB expression by $CD8^+$ T cells, both in the spleen and the primary tumor (**Fig. 5C** and **D**). Of note, transfer of $p50^{-/-}$ $CD11b^+Ly6G^-Ly6C^+$ cells did not affect tumor growth, as well as the phenotype of $CD4^+$ and $CD8^+$ T cells. These data demonstrate that accumulation of nuclear p50 in M-MDSCs promotes their suppressive functions in blunting the efficacy of cytokine-mediated immunotherapy (i.e., IFNγ). This conclusion was further strengthened observing that ablation of p50 in tumor-bearing mice improved the antitumor and antimetastatic activity of the immunostimulatory cytokine IL12 (Supplementary Fig. S5).

## Tumor-derived PGE2 primes M-MDSCs for higher IFNγ-induced NO-mediated suppressive activity

In the attempt to identify tumor-derived signals controlling nuclear p50 accumulation, we used BM-MDSCs (29) to test molecules detected

Published OnlineFirst April 7, 2020; DOI: 10.1158/0008-5472.CAN-19-2843



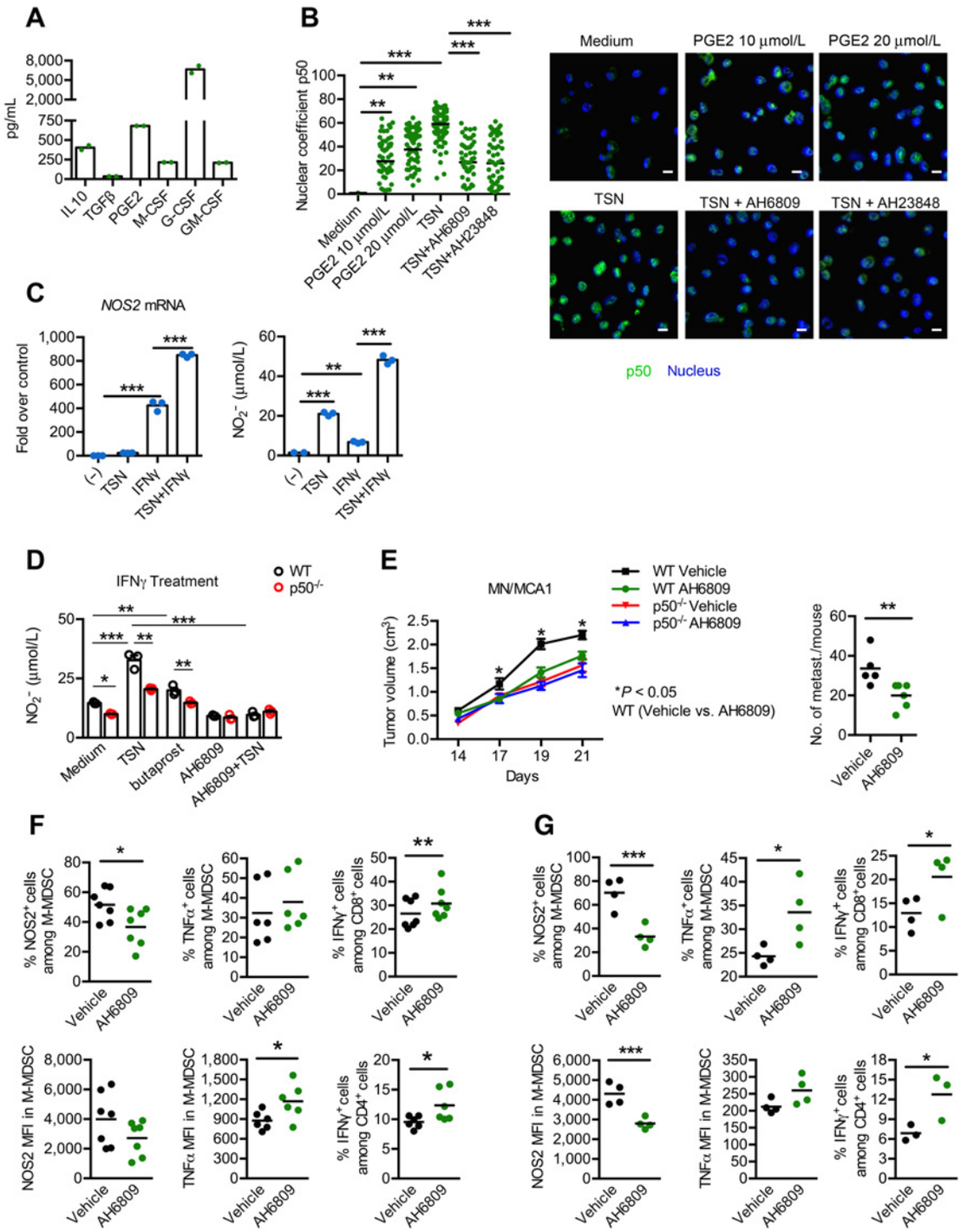


**Figure 6.**

Tumor-derived PGE2 promotes p50 NF-κB–mediated suppressive M-MDSC functions. **A,** Levels of IL10, TGFβ, PGE2, GM-CSF, G-CSF, and M-CSF in $n = 2$ independent TSN, estimated by ELISA. **B,** Right, confocal microscopy of p50 NF-κB in BM-derived M-MDSC conditioned with either TSN, PGE2 (10 μmol/L and 20 μmol/L), or TSN plus the EP2 antagonist AH6809 or the EP4 antagonist AH23848. Scale bars, 10 μm. Post 48 hours of *in vitro* activation, cells were stained with anti-p50 NF-κB antibody (green) and nuclei were counterstained with DAPI (blue). Left, confocal microscopy analysis of p50 NF-κB nuclear fluorescence intensity (**, $P < 0.01$; ***, $P < 0.001$ by two tailed one-way ANOVA; medium, $n = 34$ nuclei; PGE2, 10 μmol/L, $n = 62$ nuclei; PGE2, 20 μmol/L, $n = 71$ nuclei; TSN, $n = 96$ nuclei; TSN+AH6809, $n = 70$ nuclei; TSN+AH23848, $n = 61$ nuclei). **C,** TSN primes IFNγ-treated MDSC for enhanced expression of *NOS2* mRNA and NO production (***, $P < 0.001$ by two-tailed one-way ANOVA; $n = 3$ technical replicates of a representative experiment). **D,** In hibition of NO production by the EP2 receptor antagonist AH6809 in TSN-primed and IFNγ-treated WT and p50-deficient BM-MDSCs. (*Continued on the following page.*)

Published OnlineFirst April 7, 2020; DOI: 10.1158/0008-5472.CAN-19-2843



in the TSN (**Fig. 6A**) and reported to either induce nuclear accumulation of p50 NF-κB homodimers in macrophages (i.e., PGE2, IL10, TGFβ; ref. 10) or myeloid cell differentiation (GM-CSF, G-CSF, and M-CSF). Confocal microscopy analysis showed that neither M-, GM- nor G-CSF induced p50 accumulation (Supplementary Fig. S6A). In contrast, PGE2 efficiently induced nuclear p50, whereas the PGE2 receptor antagonists EP2 (AH6809) and EP4 (AH23848; ref. 41) inhibited the TSN-induced nuclear accumulation of p50 (**Fig. 6B**). Furthermore, BM-MDSCs primed with TSN showed higher levels of both *Nos2* mRNA and NO production in response to IFNγ (**Fig. 6C**), which was prevented by AH6809 (**Fig. 6D**). In agreement, pretreatment with Butaprost, a selective agonist of EP2, enhanced IFNγ-mediated NO production in a p50-dependent manner (**Fig. 6D**).

We next evaluated the capacity of AH6809 to interfere with the MN/MCA1 fibrosarcoma *in vivo*. Because MN-MCA1 cells also express the EP2R (Supplementary Fig. S6B), we evaluated the effects of AH6809 on tumor cell viability. MN-MCA1 cells were cultured in presence of 10 μmol/L AH6809, 10 μmol/L PGE2 or the combination of AH6809 and PGE2, up to 72 hours. As shown (Supplementary Fig. S6C), AH6809 did not affect tumor cell proliferation and viability. In contrast, daily treatment with AH6809 inhibited tumor growth (**Fig. 6E**, left) and reduced the number of lung metastasis (**Fig. 6E**, right) in WT mice. Consistently, no tumor growth inhibition was observed in $p50^{-/-}$ mice upon treatment with AH6809 (**Fig. 6E**, left). In agreement with the phenotype of $p50^{-/-}$ mice (**Fig. 3C** and **D**), flow cytometry of tumor tissue (MN/MCA1) from tumor-bearing WT mice, showed that AH6809 treatment significantly reduced the expression of NOS2 (**Fig. 6F**, left) by $CD11b^{+}Ly6G^{-}Ly6C^{+}$ cells, while increasing the expression of TNFα (**Fig. 6F**, center), as well as the $IFNγ^{+}CD4^{+}$ and $IFNγ^{+}CD8^{+}$ T cells (**Fig. 6F**, right). Similar results were obtained in splenic M-MDSCs (**Fig. 6G**). Further supporting the protumoral activity of the PGE2–p50–NO axis, *in vivo* treatment with AH6809 displayed an antitumor effects comparable with an antibody against the PD-1 immune checkpoint inhibitor (anti-PD-1), both in terms of primary tumor growth (MN/MCA1) and lung metastasis formation (Supplementary Fig. S6D), while the expression of NOS2 in $CD11b^{+}Ly6C^{+}$ WT M-MDSCs cells was reduced to levels comparable with $p50^{-/-}$ M-MDSC (Supplementary Fig S6E). In agreement, treatment of B16-bearing WT mice with AH6809 reduced tumor growth and NOS2 expression by $CD11b^{+}Ly6C^{+}$ M-MDSCs, mimicking p50 NF-κB ablation (Supplementary Fig. S6F). Despite also B16 melanoma cells expressed EP2R (Supplementary Fig. S6G), AH6809 did not elicit direct cytotoxic effects *in vitro* (Supplementary Fig. S6H), neither antitumor effects in p50-deficient mice (Supplementary Fig. S6F).

Finally, we investigated the effect of NO on the antitumor activity of IFNγ *in vivo*. WT B16-bearing mice were then treated with IFNγ and/or with L-NMMA. While treatment with IFNγ elicited poor effects on tumor growth, L-NMMA alone displayed a significant antitumor effect, which was enhanced in combination with IFNγ (**Fig. 7A**). Moreover, L-NMMA, and even more its combination with IFNγ, reduced the expression of NOS2 by tumor M-MDSCs (**Fig. 7B**, top) and enhanced the expression of TNFα (**Fig. 7B**, bottom), while increasing the number of tumor-infiltrating $IFNγ^{+}CD8^{+}$ T cells (**Fig. 7C**). These results indicate NO as a terminal mediator of suppressive myeloid cell functions and suggest that blocking the PGE2-p50-NO axis either upstream (i.e., EP2 inhibitors) or downstream (i.e., NOS2 inhibitor L-NMMA) may restore antitumor immunity.

To corroborate this finding in patients with cancer, we analyzed the expression of both the PGE2 receptor EP2 and NOS2 in PBMCs from patients with advanced colorectal cancer (stage T2/T3; $n = 5$). In agreement with mouse data, human M-MDSCs ($HLA\text{-}DR^{low/-}CD14^{+}CD33^{high}$; Supplementary Fig. S2A) expressed the PGE2 receptor EP2 (**Fig. 7D**). Moreover, human peripheral blood monocytes primed with TSN from the human pancreatic carcinoma cell line PANC1, containing 923 μg/mL of PGE2, and subsequently treated with IFNγ, showed higher levels of intracellular NOS2 protein, that were reduced by treatment with AH6809 (**Fig. 7E**). While confirming the suppressive activity of PGE2 in cancer bearers (42), our results are the first to identify the PGE2-driven nuclear accumulation of p50 NF-κB as leading event in the differentiation of suppressive M-MDSCs.

## Discussion

Cancers support a pathologic generation of immunosuppressive and tumor-promoting MDSC populations (12, 13), that share phenotypic traits with TAMs, including the expression of anti-inflammatory M2 polarized genes (10). Here, we demonstrate that tumor-derived PGE2 drives the suppressive phenotype of M-MDSCs through upregulation of nuclear p50 NF-κB, a key player in the resolution of the inflammatory response, that links unresolved cancer inflammation with tolerance (9, 28). Accumulation of nuclear p50 NF-κB, in both mouse ($CD11b^{+}Ly6G^{-}Ly6C^{+}$) and human (patients with colorectal cancer; $CD14^{+}HLA\text{-}DR^{low/-}$) M-MDSCs, diverts their transcriptional responses to IFNγ toward enhanced production of the immunosuppressive molecule NO. Consistently, ablation of p50 NF-κB reactivated specific antitumor immunity and reinstated the *in vivo* antitumor activity of IL12 and IFNγ, two immunostimulatory cytokines evaluated in clinical trials against various human tumors (e.g., colorectal cancer, soft tissue sarcoma, melanoma, and plasma cell neoplasms; ref. 16). This observation provides new insights into the ambivalent action of IFNγ (22, 43, 44), which in clinical protocols has shown either moderate or poor efficacy (17, 21, 45). This ambiguity is reminiscent of the bimodal immunologic activities of IFNγ, which promotes transcription of genes involved in the activation of immune responses (e.g. MHC class I and class II, IL12; ref. 46) and simultaneously induces immunosuppressive pathways, including B7-H1 (47, 48) and the immunosuppressive enzymes IDO (23) and iNOS/NOS2 (12, 13). The biological activity of IFNγ requires

(*Continued.*) Both TSN and the selective EP2 agonist (butaprost) displayed priming activity for NO production in WT BM-MDSC, but not in the p50-deficient counterpart (**, $P < 0.01$; ***, $P < 0.001$ by two-tailed one-way ANOVA; $n = 3$ technical replicates of a representative experiment). **E,** Left, AH6809 inhibits fibrosarcoma growth (data shown are mean±SEM; *, $P < 0.05$ by two-tailed two-way ANOVA; $n = 6$ WT vehicle mice; $n = 6$ WT AH6809–treated mice; $n = 6$ $p50^{-/-}$ vehicle mice; $n = 6$ $p50^{-/-}$ AH6809–treated mice) and lung metastasis formation in tumor-bearing WT mice (**, $P < 0.01$ by two-tailed *t* test; $n = 5$ WT vehicle-treated mice; $n = 6$ WT AH6809-treated mice). **F** and **G,** FACS analysis of infiltrating immune cells in tumor (**F**) and spleen (**G**) of fibrosarcoma (MN/MCA1)-bearing WT mice treated with AH6809 or untreated (vehicle). We evaluated expression of NOS2 and TNFα in M-MDSCs and IFNγ in $CD4^{+}$ and $CD8^{+}$ T cells. Data pooled from two different experiments are shown. *, $P < 0.05$; **, $P < 0.01$ by two-tailed *t* test. Tumor, TNFα in M-MDSC, $n = 6$ WT vehicle and $n = 6$ WT AH6809–treated mice; NOS2 in M-MDSC, $n = 7$ WT vehicle and $n = 7$ WT AH6809–treated mice; IFNγ in $CD4^{+}$ T cells, $n = 6$ WT vehicle and $n = 6$ WT AH6809–treated mice; IFNγ in $CD8^{+}$ T cells, $n = 7$ WT vehicle and $n = 7$ WT AH6809–treated mice. Spleen, NOS2, and TNFα in M-MDSC and IFNγ in $CD8^{+}$ T cells, $n = 4$ WT vehicle and $n = 4$ WT AH6809–treated mice; IFNγ in $CD4^{+}$ T cells, $n = 3$ WT vehicle and $n = 3$ WT AH6809–treated mice.

Published OnlineFirst April 7, 2020; DOI: 10.1158/0008-5472.CAN-19-2843



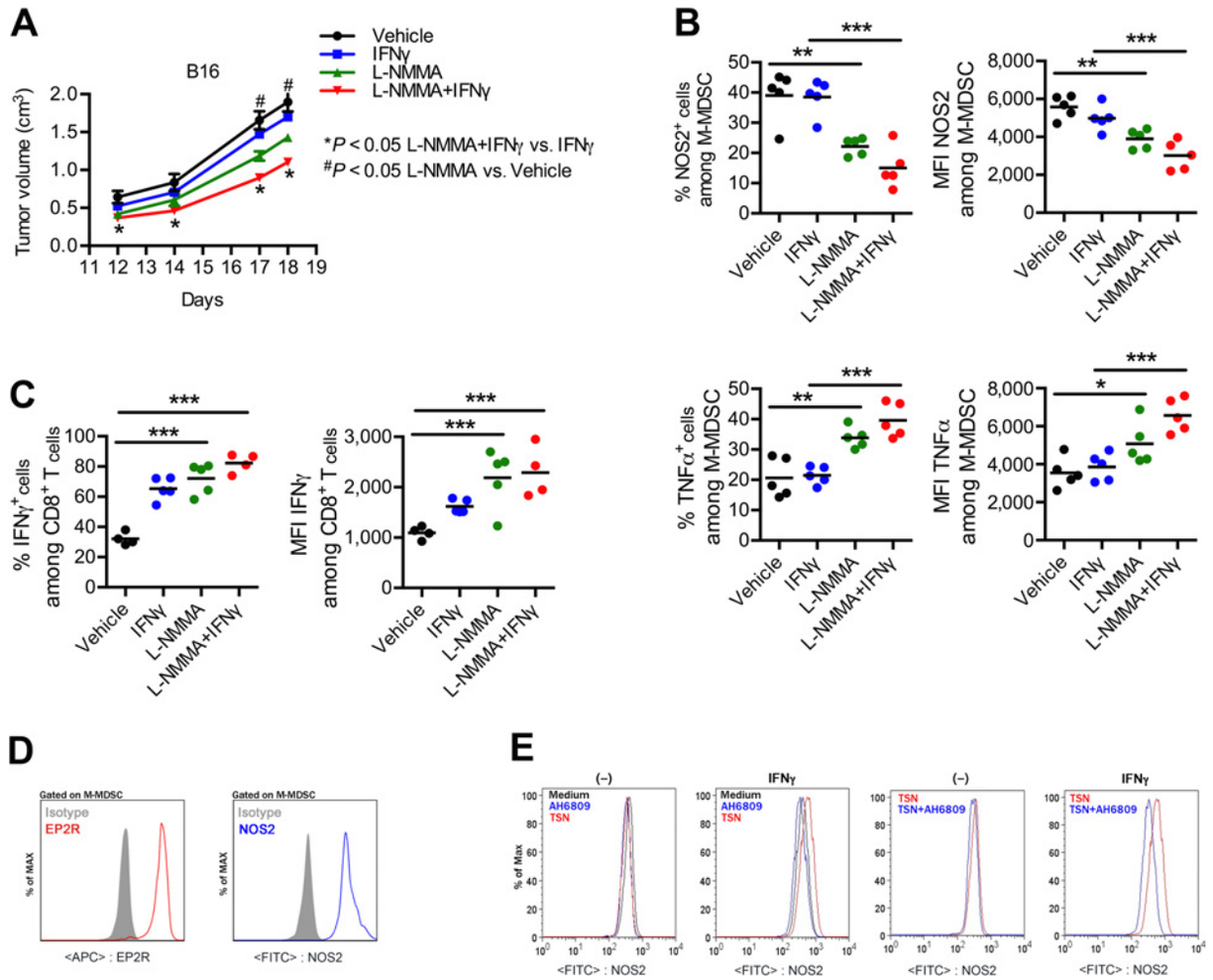


**Figure 7.**

Blocking NO production restores the antitumor activity of IFNγ *in vivo*. **A,** L-NMMA treatment reduces melanoma (B16) growth in WT mice and releases the antitumor activity of IFNγ (data shown are mean ± SEM; *P* value was calculated by two-tailed two-way ANOVA; $n = 5$ WT vehicle–treated mice; $n = 5$ IFNγ-treated mice; $n = 5$ L-NMMA–treated mice; $n = 5$ IFNγ + L-NMMA–treated mice). **B,** L-NMMA reduces the expression of NOS2 (top) and increases the expression of TNFα (bottom) in tumor-infiltrating M-MDSCs (*, $P < 0.05$ by two-tailed one-way ANOVA; $n = 5$ WT vehicle–treated mice; $n = 5$ IFNγ-treated mice; $n = 5$ L-NMMA–treated mice; $n = 5$ IFNγ + L-NMMA–treated mice). **C,** L-NMMA enhances tumor infiltration of IFNγ-expressing $CD8^+$ T cells. *, $P < 0.05$ by two-tailed one-way ANOVA; $n = 4$ WT vehicle–treated mice; $n = 5$ IFNγ-treated mice; $n = 5$ L-NMMA–treated mice; $n = 4$ IFNγ + L-NMMA–treated mice. **D,** Representative flow cytometry of EP2 receptor and NOS2 expression in peripheral blood M-MDSCs from patients with colorectal cancer ($n = 5$ patients with colorectal cancer). **E,** Flow cytometry analysis of NOS2 in IFNγ-treated human peripheral blood monocytes primed with TSN from the human pancreatic carcinoma cell line PANC1 in the presence or absence of the EP2 antagonist AH6809.

the nuclear translocation and the DNA binding of the STAT1 homodimer to gamma activated sequence (GAS) sites on the promoters of downstream target genes (49), including Nos2 (50). Accumulation of p50 NF-κB in myeloid cells does not affect IFNγ-dependent STAT1 phosphorylation, but rather controls their chromatin landscape to promote binding of STAT1 onto specific gene regulatory elements of IFNγ-responsive genes, including *Nos2*. We also observed that lack of p50 results in increased $CD11b^+Ly6G^-Ly6C^+$ cells in the spleen of tumor-bearing mice, with low NO production and suppressive activity, as well as in the preferential skewing of HSCs toward the monocytic branch in the bone marrow. This hematopoietic output is in agreement with the $Irf8^{high}$ feature that we observed in p50-deficient PMN-MDSCs, because IRF8 is a cell fate–switching factor driving terminal differentiation of the monocytic lineage (36) ad preventing MDSC expansion (35).

COX2-stimulated production of PGE2 enhances the expansion of MDSCs and promotes suppression of adaptive immunity (51). We show that antagonists of the PGE2 receptors EP1/EP2 reprogram M-MDSC functions in response to IFNγ toward an inflammatory phenotype (i.e., $NOS2^{low}/TNF^{high}$), associated with increased specific antitumor immunity. Of relevance, in analogy with the results obtained both with the inhibition of PGE2 receptors and with the ablation of the NF-κB p50 gene, the NOS L-NMMA inhibitor reprogrammed the M-MDSCs toward an $NOS2^{low}/TNF\alpha^{high}$ phenotype, associated with an increased antitumoral effect of IFNγ. This evidence indicates the gasotransmitter NO (52) as the final effector of the protumoral reprogramming of myeloid cells, guided by the PGE2/p50 axis.

COX inhibitors (e.g., aspirin) were suggested for prevention and treatment of cancer (42). Nevertheless, due to their severe side effects, targeting specific prostanoid receptors endowed with immunosuppressive properties, such as EP2 (53–55), might provide an alternative selective and safer approach to burst specific immunity in cancer patients. Our work indicates that p50 NF-κB accumulation diverts the differentiation and activation status of myeloid cells, leading to the resolution of immune and inflammatory responses. It further demonstrates that in cancer an accumulation of p50 NF-κB, induced by PGE2, acts as an epigenetic hacker of M-MDSC functions, which establishes their suppressive phenotype, suggesting the use of PGE2 receptor antagonists as potential adjuvants for anticancer immunotherapy.

## Disclosure of Potential Conflicts of Interest

V. Bronte has ownership interest (including patents) in Xios Therapeutics, Codiak BioSciences, EMD Serono, and BioNTech AG and is a consultant/advisory board member for Xios Therapeutics, Codiak BioSciences, EMD Serono, Incyte Corporation, and Ganymed Pharmaceuticals AG. F. Balzac is a consultant at KITHER. E. Hirsch is a consultant/advisory board member for Kither Biotech. No potential conflicts of interest were disclosed by the other authors.

## Authors' Contributions

**Conception and design:** P. Larghi, V. Bronte, A. Sica
**Development of methodology:** S. Morlacchi, A. Bleve, M.G. Totaro, P. Larghi, M. Rimoldi, L. Strauss, M. Storto, A. Ippolito, A. Doni, R. Ostuni, V. Bronte
**Acquisition of data (provided animals, acquired and managed patients, provided facilities, etc.):** C. Porta, F.M. Consonni, S. Sangaletti, A. Bleve, M. Storto, T. Pressiani, L. Rimassa, S. Tartari, A. Ippolito, A. Doni, R. Ostuni, F. Balzac, E. Turco, E. Hirsch
**Analysis and interpretation of data (e.g., statistical analysis, biostatistics, computational analysis):** C. Porta, C. Tripodo, L. Strauss, A. Ippolito, G. Soldà, S. Duga, V. Piccolo, R. Ostuni, G. Natoli, A. Sica
**Writing, review, and/or revision of the manuscript:** C. Porta, L. Rimassa, G. Soldà, S. Duga, V. Bronte, M.P. Colombo, A. Sica
**Study supervision:** G. Natoli, A. Sica
**Other (performed the experiments):** S. Morlacchi
**Other (performed some experiments):** S. Banfi
**Other (acquisitions of confocal optical microscopy and colocalization analysis):** A. Doni

## Acknowledgments

This work was supported by Associazione Italiana per la Ricerca sul Cancro (AIRC) Italy (12810, to S. Sangaletti; IG numbers 10137 to M.P. Colombo; IG numbers 15585, 19885 to A. Sica; AIRC 5 per Mille, number 22757 to A. Sica; AIRC 5 per Mille, Program Innovative Tools for Cancer Risk Assessment and Diagnosis, number 12162 to C. Tripodo; Three-Year fellowship "Pierluigi Meneghelli," project code 19682, to F.M. Consonni). Ministero dell'istruzione, dell'Università e della Ricerca (MIUR), Italy (PRIN 2015YYKPNN and 2017BA9LM5_001 to A. Sica); Ministero della Salute, Ricerca Finalizzata RF-2016-0236842 to A. Sica and GR-2013-02355637 to S. Sangaletti; European Research Council (ERC) Advanced grant ERCAdGN.692789 to G. Natoli; Fondazione Cariplo 2016/0871 to A. Sica, Associazione "Augusto per la Vita," Novellara, Italy, to A. Sica, Associazione "Medicine Rocks," Milan, Italy, to A. Sica, and Università del Piemonte Orientale, Novara, Italy, Ricerca locale 2019 to C. Porta.

The costs of publication of this article were defrayed in part by the payment of page charges. This article must therefore be hereby marked *advertisement* in accordance with 18 U.S.C. Section 1734 solely to indicate this fact.

Received September 11, 2019; revised February 28, 2020; accepted April 2, 2020; published first April 7, 2020.

## References

1. Mosser DM, Edwards JP. Exploring the full spectrum of macrophage activation. Nat Rev Immunol 2008;8:958–69.
2. Sica A, Mantovani A. Macrophage plasticity and polarization: in vivo veritas. J Clin Invest 2012;122:787–95.
3. Mantovani A, Sozzani S, Locati M, Allavena P, Sica A. Macrophage polarization: tumor-associated macrophages as a paradigm for polarized M2 mononuclear phagocytes. Trends Immunol 2002;23:549–55.
4. Mantovani A, Sica A. Macrophages, innate immunity and cancer: balance, tolerance, and diversity. Curr Opin Immunol 2010;22:231–7.
5. Mantovani A, Allavena P, Sica A, Balkwill F. Cancer-related inflammation. Nature 2008;454:436–44.
6. Martinez FO, Helming L, Gordon S. Alternative activation of macrophages: an immunologic functional perspective. Annu Rev Immunol 2009;27:451–83.
7. Noy R, Pollard JW. Tumor-associated macrophages: from mechanisms to therapy. Immunity 2014;41:49–61.
8. Ziegler-Heitbrock HW, Petersmann I, Frankenberger M. p50 (NF-kappa B1) is upregulated in LPS tolerant P388D1 murine macrophages. Immunobiology 1997;198:73–80.
9. Porta C, Rimoldi M, Raes G, Brys L, Ghezzi P, Di Liberto D, et al. Tolerance and M2 (alternative) macrophage polarization are related processes orchestrated by p50 nuclear factor kappaB. Proc Natl Acad Sci U S A 2009;106:14978–83.
10. Biswas SK, Gangi L, Paul S, Schioppa T, Saccani A, Sironi M, et al. A distinct and unique transcriptional program expressed by tumor-associated macrophages (defective NF-kappaB and enhanced IRF-3/STAT1 activation). Blood 2006;107:2112–22.
11. Strauss L, Sangaletti S, Consonni FM, Szebeni G, Morlacchi S, Totaro MG, et al. RORC1 regulates tumor-promoting "Emergency" granulo-monocytopoiesis. Cancer Cell 2015;28:253–69.
12. Sica A, Bronte V. Altered macrophage differentiation and immune dysfunction in tumor development. J Clin Invest 2007;117:1155–66.
13. Gabrilovich DI, Ostrand-Rosenberg S, Bronte V. Coordinated regulation of myeloid cells by tumours. Nat Rev Immunol 2012;12:253–68.
14. Martin F, Apetoh L, Ghiringhelli F. Role of myeloid-derived suppressor cells in tumor immunotherapy. Immunotherapy 2012;4:43–57.
15. Zaidi MR, Davis S, Noonan FP, Graff-Cherry C, Hawley TS, Walker RL, et al. Interferon-gamma links ultraviolet radiation to melanomagenesis in mice. Nature 2011;469:548–53.
16. Vacchelli E, Galluzzi L, Eggermont A, Galon J, Tartour E, Zitvogel L, et al. Trial watch: immunostimulatory cytokines. Oncoimmunology 2012;1:493–506.
17. Miller CH, Maher SG, Young HA. Clinical use of interferon-gamma. Ann N Y Acad Sci 2009;1182:69–79.
18. Assi HI, Kamphorst AO, Moukalled NM, Ramalingam SS. Immune checkpoint inhibitors in advanced non-small cell lung cancer. Cancer 2018;124:248–61.
19. Lo Russo G, Moro M, Sommariva M, Cancila V, Boeri M, Centonze G, et al. Antibody-Fc/FcR interaction on macrophages as a mechanism for hyperprogressive disease in non-small cell lung cancer subsequent to PD-1/PD-L1 blockade. Clin Cancer Res 2019;25:989–99.
20. Adams DO, Hamilton TA. The cell biology of macrophage activation. Annu Rev Immunol 1984;2:283–318.
21. Zaidi MR, Merlino G. The two faces of interferon-gamma in cancer. Clin Cancer Res 2011;17:6118–24.
22. Dighe AS, Richards E, Old LJ, Schreiber RD. Enhanced in vivo growth and resistance to rejection of tumor cells expressing dominant negative IFN gamma receptors. Immunity 1994;1:447–56.
23. Pallotta MT, Orabona C, Volpi C, Vacca C, Belladonna ML, Bianchi R, et al. Indoleamine 2,3-dioxygenase is a signaling protein in long-term tolerance by dendritic cells. Nat Immunol 2011;12:870–8.
24. Kondo A, Yamashita T, Tamura H, Zhao W, Tsuji T, Shimizu M, et al. Interferon-gamma and tumor necrosis factor-alpha induce an immunoinhibitory molecule, B7-H1, via nuclear factor-kappaB activation in blasts in myelodysplastic syndromes. Blood 2010;116:1124–31.
25. Topalian SL, Drake CG, Pardoll DM. Immune checkpoint blockade: a common denominator approach to cancer therapy. Cancer Cell 2015;27:450–61.
26. Chan SR, Vermi W, Luo J, Lucini L, Rickert C, Fowler AM, et al. STAT1-deficient mice spontaneously develop estrogen receptor alpha-positive luminal mammary carcinomas. Breast Cancer Res 2012;14:R16.
27. Saccani A, Schioppa T, Porta C, Biswas SK, Nebuloni M, Vago L, et al. p50 nuclear factor-kappaB overexpression in tumor-associated macrophages

Published OnlineFirst April 7, 2020; DOI: 10.1158/0008-5472.CAN-19-2843



inhibits M1 inflammatory responses and antitumor resistance. Cancer Res 2006; 66:11432–40.
28. Porta C, Ippolito A, Consonni FM, Carraro L, Celesti G, Correale C, et al. Protumor steering of cancer inflammation by p50 NF-kappaB enhances colorectal cancer progression. Cancer Immunol Res 2018;6:578–93.
29. Marigo I, Bosio E, Solito S, Mesa C, Fernandez A, Dolcetti L, et al. Tumor-induced tolerance and immune suppression depend on the C/EBPbeta transcription factor. Immunity 2010;32:790–802.
30. Ostuni R, Natoli G. Lineages, cell types and functional states: a genomic view. Curr Opin Cell Biol 2013;25:759–64.
31. Garber M, Yosef N, Goren A, Raychowdhury R, Thielke A, Guttman M, et al. A high-throughput chromatin immunoprecipitation approach reveals principles of dynamic gene regulation in mammals. Mol Cell 2012;47:810–22.
32. Movahedi K, Guilliams M, Van den Bossche J, Van den Bergh R, Gysemans C, Beschin A, et al. Identification of discrete tumor-induced myeloid-derived suppressor cell subpopulations with distinct T cell-suppressive activity. Blood 2008;111:4233–44.
33. Mandruzzato S, Solito S, Falisi E, Francescato S, Chiarion-Sileni V, Mocellin S, et al. IL4Ralpha+ myeloid-derived suppressor cell expansion in cancer patients. J Immunol 2009;182:6562–8.
34. Wang D, Paz-Priel I, Friedman AD. NF-kappa B p50 regulates C/EBP alpha expression and inflammatory cytokine-induced neutrophil production. J Immunol 2009;182:5757–62.
35. Waight JD, Netherby C, Hensen ML, Miller A, Hu Q, Liu S, et al. Myeloid-derived suppressor cell development is regulated by a STAT/IRF-8 axis. J Clin Invest 2013;123:4464–78.
36. Friedman AD. Transcriptional control of granulocyte and monocyte development. Oncogene 2007;26:6816–28.
37. El Kasmi KC, Qualls JE, Pesce JT, Smith AM, Thompson RW, Henao-Tamayo M, et al. Toll-like receptor-induced arginase 1 in macrophages thwarts effective immunity against intracellular pathogens. Nat Immunol 2008;9:1399–406.
38. Sica A, Saccani A, Bottazzi B, Polentarutti N, Vecchi A, van Damme J, et al. Autocrine production of IL-10 mediates defective IL-12 production and NF-kappa B activation in tumor-associated macrophages. J Immunol 2000;164: 762–7.
39. Platanias LC. Mechanisms of type-I- and type-II-interferon-mediated signalling. Nat Rev Immunol 2005;5:375–86.
40. Dinapoli MR, Calderon CL, Lopez DM. The altered tumoricidal capacity of macrophages isolated from tumor-bearing mice is related to reduce expression of the inducible nitric oxide synthase gene. J Exp Med 1996;183:1323–9.
41. Zhang T, Gong X, Hu G, Wang X. EP2-PKA signaling is suppressed by triptolide in lipopolysaccharide-induced microglia activation. J Neuroinflammation 2015; 12:50.
42. Zelenay S, van der Veen AG, Bottcher JP, Snelgrove KJ, Rogers N, Acton SE, et al. Cyclooxygenase-dependent tumor growth through evasion of immunity. Cell 2015;162:1257–70.
43. Kaplan DH, Shankaran V, Dighe AS, Stockert E, Aguet M, Old LJ, et al. Demonstration of an interferon gamma-dependent tumor surveillance system in immunocompetent mice. Proc Natl Acad Sci U S A 1998;95:7556–61.
44. Shankaran V, Ikeda H, Bruce AT, White JM, Swanson PE, Old LJ, et al. IFNgamma and lymphocytes prevent primary tumour development and shape tumour immunogenicity. Nature 2001;410:1107–11.
45. Wilke CM, Wei S, Wang L, Kryczek I, Kao J, Zou W. Dual biological effects of the cytokines interleukin-10 and interferon-gamma. Cancer Immunol Immunother 2011;60:1529–41.
46. Lawrence T, Natoli G. Transcriptional regulation of macrophage polarization: enabling diversity with identity. Nat Rev Immunol 2011;11:750–61.
47. Curiel TJ, Wei S, Dong H, Alvarez X, Cheng P, Mottram P, et al. Blockade of B7-H1 improves myeloid dendritic cell-mediated antitumor immunity. Nat Med 2003;9:562–7.
48. Wu K, Kryczek I, Chen L, Zou W, Welling TH. Kupffer cell suppression of CD8+ T cells in human hepatocellular carcinoma is mediated by B7-H1/programmed death-1 interactions. Cancer Res 2009;69:8067–75.
49. Platanias LC. Introduction: interferon signals: what is classical and what is nonclassical? J Interferon Cytokine Res 2005;25:732.
50. Ganster RW, Taylor BS, Shao L, Geller DA. Complex regulation of human inducible nitric oxide synthase gene transcription by Stat 1 and NF-kappa B. Proc Natl Acad Sci U S A 2001;98:8638–43.
51. Mao Y, Sarhan D, Steven A, Seliger B, Kiessling R, Lundqvist A. Inhibition of tumor-derived prostaglandin-e2 blocks the induction of myeloid-derived suppressor cells and recovers natural killer cell activity. Clin Cancer Res 2014;20: 4096–106.
52. Kobayashi Y. The regulatory role of nitric oxide in proinflammatory cytokine expression during the induction and resolution of inflammation. J Leukoc Biol 2010;88:1157–62.
53. Ganesh T. Prostanoid receptor EP2 as a therapeutic target. J Med Chem 2014;57: 4454–65.
54. O'Brien AJ, Fullerton JN, Massey KA, Auld G, Sewell G, James S, et al. Immunosuppression in acutely decompensated cirrhosis is mediated by prostaglandin E2. Nat Med 2014;20:518–23.
55. O'Callaghan G, Houston A. Prostaglandin E2 and the EP receptors in malignancy: possible therapeutic targets? Br J Pharmacol 2015;172:5239–50.

Published OnlineFirst April 7, 2020; DOI: 10.1158/0008-5472.CAN-19-2843

Cancer Research
The Journal of Cancer Research (1916–1930) | The American Journal of Cancer (1931–1940)

AACR American Association for Cancer Research

# Tumor-Derived Prostaglandin E2 Promotes p50 NF-κB-Dependent Differentiation of Monocytic MDSCs

Chiara Porta, Francesca Maria Consonni, Sara Morlacchi, et al.

*Cancer Res* 2020;80:2874-2888. Published OnlineFirst April 7, 2020.